Oral antigen exposure under co-stimulation blockade generates Treg cells to establish immune tolerance despite prior sensitization

Masaya Arai[1]*, Ryoji Kawakami[1,2]*, Yamami Nakamura[1], Yoko Naito[3], Daisuke Motooka[3], Atsushi Sugimoto[1], Tomiko Kimoto[1], Naganari Ohkura[1,4], Norihisa Mikami[1], and Shimon Sakaguchi[1,2]†

[1] Department of Experimental Immunology, Immunology Frontier Research Center, The University of Osaka, 3-1, Yamadaoka, 565-0871, Suita, Osaka, Japan
[2] Department of Experimental Immunology, Institute for Life and Medical Sciences, Kyoto University, Sakyo-ku, 606-8507 Kyoto, Japan
[3] Genome Information Research Center, Research Institute for Microbial Diseases, The University of Osaka, 3-1, Yamadaoka, 565-0871, Suita, Osaka, Japan
[4] Department of Frontier Research in Tumor Immunology, Graduate School of Medicine, The University of Osaka, 3-1, Yamadaoka, 565-0871, Suita, Osaka, Japan
* These authors contributed equally to this work
† Corresponding author. Email: shimon@ifrec.osaka-u.ac.jp (S.S.)

Abstract

Antigen-specific oral tolerance is effective in preventing harmful immune responses in antigen-non-sensitized animals but difficult to be induced in those already antigen-primed. Here, we show in mice that feeding of antigen-containing diet generates peripherally derived regulatory T (pTreg) cells that exhibit a tissue-adapted effector phenotype. The antigen feeding also enables the generated pTreg cells to acquire Treg-specific epigenomic changes in Treg signature genes including *Foxp3*, hence the stability of Treg-specific function. Cessation of antigen feeding, however, results in decline in oral tolerance with diminution of pTreg cells. Transcriptomic analysis has revealed that the induced pTreg cells predominantly express CD101. $CD101^+$ Treg cells with a similar phenotype and epigenetic alterations can also be generated *in vitro* from antigen-primed naïve $CD4^+$ T cells by blockade of CD28-mediated co-stimulation during TGF-β-dependent Treg induction. Furthermore, *in vivo* CD28 signal blockade by CTLA-4-immunoglobulin fusion protein (CTLA4-Ig) before antigen feeding can establish oral tolerance in the mice precedingly antigen-sensitized by a non-oral route. The blockade facilitates differentiation of antigen-specific conventional T cells into $CD101^+$ pTreg cells. Thus, continuous oral antigen administration combined with CD28 co-stimulation blockade generates $CD101^+$ antigen-specific functionally stable pTreg cells, which can establish long-term systemic antigen-specific immune tolerance even in antigen-pre-sensitized animals.

Introduction

Oral tolerance is antigen-specific systemic immunological unresponsiveness induced by intestinal exposure to antigens derived from ingested food or commensal microbes (Chase, 1946; Cerovic et al., 2024). It is effective in preventing autoimmune diseases (e.g., arthritis, diabetes, and multiple sclerosis) and allergies (e.g., food allergy) in animal models (Rezende and Weiner, 2022). In humans, early exposure to peanut protein is reportedly capable of preventing peanut allergy in children (Du Toit et al., 2015, 2024). However, it has not been significantly successful in humans to induce oral tolerance for treating ongoing immunological diseases such as chronic allergy and autoimmune disease (Faria and Weiner, 2005). It is therefore a long outstanding issue to determine how harmful immune responses that have been already triggered and chronically progressing can be halted and cured by inducing antigen-specific oral tolerance (Mowat, 2018).

Naturally occurring $CD4^+$ regulatory T (nTreg) cells expressing the transcription factor Foxp3, including thymus-derived Treg (tTreg) cells and peripherally derived Treg (pTreg) cells, are indispensable for the induction and maintenance of immunological tolerance, including oral tolerance, and instrumental in controlling immunological diseases (Sakaguchi et al., 2020; Mucida et al., 2005; Josefowicz et al., 2012; Tanoue et al., 2016; Hong et al., 2022). It remains obscure, however, how antigen-specific pTreg cells are generated and how they establish and maintain oral tolerance (Cerovic et al., 2024). It has been suggested that, following antigen transportation through the intestinal epithelial cells, antigen-presenting cells (APCs), conventional dendritic cells (cDCs) in particular, play a pivotal role in the generation of antigen cognate pTreg cells in mesenteric lymph nodes (mLNs) and lymphoid tissues in the intestine (Mazzini et al., 2014; Hadis et al., 2011; Esterházy et al., 2016). Intestinal cDCs can efficiently convert TGF-β into its active form, and vitamin A into retinoic acid (RA); TGF-β and RA synergistically induce intestinal pTreg cells upon antigen stimulation (Mucida et al., 2007; Sun et al., 2007; Coombes et al., 2007). These pTreg-inducing cDCs appear to be immature DCs with low expression of the costimulatory molecules CD80 and CD86 (Morelli and Thomson, 2007; Benson et al., 2007; Lutz et al., 2021). However, the roles of CD28-mediated co-stimulation for pTreg generation and oral tolerance have not been well characterized. Addressing the issue, we have recently shown that *in vitro* antigen stimulation of $CD4^+$ conventional T (Tconv) (i.e., $CD4^+CD25^-Foxp3^-$) cells in the presence of TGF-β and IL-2 but without CD28 signal is able to efficiently induce Foxp3 Treg cells equipped with Treg-specific epigenetic changes, hence Treg cell-lineage stability, and that such functionally stable *in vitro* induced Treg (iTreg) cells can be generated not only from naïve (i.e., $CD4^+CD25^-Foxp3^-CD62L^{hi}CD44^{lo}$) but also from effector/memory (i.e., $CD4^+CD25^-Foxp3^-CD62L^{lo}CD44^{hi}$) Tconv cells (Mikami et al., 2020). The question then arises whether such *in vitro* generation of iTreg cells functionally similar to nTreg cells shares a common developmental basis with *in vivo* pTreg generation, especially in the context of oral tolerance.

Here, we have attempted to determine whether a functionally and phenotypically distinct type of pTreg cells are generated upon antigen exposure via the oral route, how they survive upon antigen stimulation and maintain their function to sustain oral tolerance, and how they can be exploited to establish robust oral tolerance not only in antigen-nonsensitized naïve mice but also in those that have been already antigen primed at other sites of the body.

Results

pTreg generation and maintenance by continuous antigen feeding and failure in establishing oral tolerance by prior antigen sensitization.

To analyze the development of pTreg cells by distinguishing them from tTreg cells, we used OVA-specific DO11.10 (DO) TCR transgenic mice that were made Rag2-deficient and expressing Foxp3-eGFP reporter gene. DO Rag2KO Foxp3-eGFP mice thus produced are hereafter abbreviated as DORe mice. Foxp3$^+$ (i.e., GFP$^+$) cells were absent in the thymus, very few in the spleen and lymph nodes including mLNs in untreated DORe mice (see also below). To determine the effects of OVA feeding on anti-OVA T-cell responses in DORe mice, we kept feeding them for 4 weeks with the diet containing egg white powder (EWP) as 10% of the protein content or with control normal chow (NC), and assessed ear swelling after 4 times of tape stripping (TS) and papain/OVA treatment on the right ear and control TS/papain treatment on the left ear (**Fig. 1A**). Compared with NC-fed mice, which showed in the right ears severe ear swelling and histologically evident inflammation in the epidermis and dermis with abundant cellular infiltration, EWP-fed mice exhibited much lower degrees of ear swelling and histologically evident inflammation (**Fig. 1B** and **1C**). They had much smaller numbers of DO CD4$^+$ T cells (**Fig. S1A**) and much lower ratios of IFN-γ, IL-4, or IL-17A-producing DO CD4$^+$ T cells in the draining lymph nodes (dLNs) (**Fig. S1B**). They developed pTreg cells in mLNs, dLNs, and the right ear in much higher ratios compared with NC-fed mice (**Fig. 1D**). Treg cells were found to be present in the spleen and also in the control left ear as well at high ratios, although in small numbers (**Fig. S1C** and **1D**), with no significant ear swelling or inflammation in EWP-fed mice (Fig. **S1D** and **S1E**). In addition, Diphtheria toxin (DTx) treatment of EWP-fed DO11.10 Rag2KO Foxp3-DTR-GFP (DORF) mice expressing the diphtheria toxin receptor (DTR) specifically in pTreg cells (**Fig. 1E**) depleted them in the OVA-challenged ear and dLNs. It evoked severe ear swelling and inflammation (**Fig. 1F** and **1G**) with significant increases of inflammatory cytokine-producing T cells especially in the ear and dLNs (**Fig. S1F** and **S1G**).

To determine whether induction of oral tolerance would require continuous antigen exposure, we ceased EWP feeding for 4 or 8 weeks before the OVA challenge to the ear (**Fig. 1H**). Despite prior EWP feeding for 4 weeks, the feeding-suspended DORe mice showed ear inflammation as severe as control NC-fed mice (**Fig. 1I**), reduced ratios of pTreg cells, and increased cytokine-producing T cells in the ear tissue and dLNs when compared to DORe mice that had been kept EWP-fed until the ear testing (**Fig. 1J, S1H,** and **S1I**).

Next, to examine whether antigen-specific oral tolerance could be induced in precedingly antigen-primed mice, we first sensitized DORe mice by TS/papain/OVA treatment and then fed the mice with EWP or NC (**Fig. 1K**). Both groups developed similar degrees of ear swelling and inflammation (**Fig. 1L**). The frequencies of pTreg cells and Tconv cells producing inflammatory cytokines were comparable in mLNs, dLNs, and the ear tissues in both groups (**Fig. 1M, S1J,** and **S1K**). Moreover, the EWP-fed group showed significant body weight loss (**Fig. 1N**), indicating elicitation of systemic inflammation by oral antigen feeding in antigen-sensitized mice.

Collectively, continuous feeding of the diet containing protein antigen establishes antigen-specific oral tolerance by generating pTreg cells from antigen-specific Tconv cells. The generated pTreg

113 cells migrate through the whole body to various tissues. However, prior antigen sensitization at other
114 sites or discontinuity of antigen feeding hampers oral tolerance induction and may even evoke an
115 aberrant immune response upon antigen feeding.

116 **Antigen-dependent development of pTreg cells with Treg type epigenome in oral tolerance.**
117 To examine how the quality and quantity of antigens contained in the diet would affect the development
118 and immunological characteristics of pTreg cells in oral tolerance, we fed DORe mice with the chow
119 containing various concentrations of EWP, antigen-free AIN-93G chow containing only casein as
120 protein (Reeves et al., 1993), or NC, starting from 2 weeks of age before weaning. EWP feeding
121 increased the frequency of pTreg cells in mLNs and the small intestine lamina propria (SI-LP) in an
122 antigen dose-dependent manner, even if antigen-containing chow was taken *ad libitum* (**Fig. 2A** and **2B**).
123 High doses of EWP increased CD25 expression by the pTreg cells induced in SI-LP (**Fig. 2A** and **2C**),
124 indicating their enhanced activation status (Miyara et al., 2009). The EWP-induced pTreg cells were
125 also maintained as $CD44^{hi}CD62L^{lo}$ effector/memory type T cells in SI-LP (**Fig. S2A** and **S2B**). These
126 pTregs exhibited Treg-specific epigenetic modifications, including DNA hypomethylation at Treg
127 signature gene loci, such as *Foxp3*-conserved non-coding sequence 2 (CNS2) region and other regions
128 in *Ikzf2*, *Ikzf4*, and *Ctla4* loci (Ohkura et al., 2012) (**Fig. 2D**). By chromatin immunoprecipitation
129 sequencing (ChIP-seq) of the genomic regions associated with histone H3 Lys27 acetylation (H3K27ac)
130 as an indicator of active enhancer status, differential peak analysis revealed that Treg-specific enhancer
131 regions were activated in pTreg cells from EWP-fed DORe mice, whereas Tconv-specific enhancer
132 regions were not, as in nTreg cells in WT mice (Kitagawa et al., 2017; Kawakami et al., 2021; Dikiy et
133 al., 2021) (**Fig. 2E**). The pTreg cells thus generated had activated Treg-specific super-enhancers at the
134 *Foxp3* gene locus and other Treg signature gene loci including *Ikzf2*, *Ikzf4*, *Ctla4*, and *Il2ra* as observed
135 in WT-nTreg cells (Kitagawa et al., 2017) (**Fig. 2F** and **2G**). ATAC-seq further confirmed chromatin
136 remodeling also in these loci (**Fig. 2F** and **2G**).

137 In the experiments in Fig. 2A, we noted that NC-fed mice also possessed detectable numbers of
138 pTreg cells in mLNs and SI-LP in particular, at higher frequencies than antigen-free- or 0% EWP chow-
139 fed mice (**Fig. 2A** and **2B**). To analyze the finding, we compared pTreg development in DORe and WT
140 mice after NC feeding, and found that the former developed $Foxp3^{+}$ cells at higher ratios than the latter
141 in SI-LP, the large intestine lamina propria (LI-LP), and among small intestine intraepithelial (SI-IE)
142 cells, but not in the spleen and LNs (**Fig. S2C** and **S2D**). The $Foxp3^{+}$ cells in NC-fed DORe mice
143 exhibited DNA hypomethylation at Treg-specific demethylation regions in Treg signature genes (**Fig.**
144 **S2F**), and expressed Helios and Neuropilin-1 (**Fig. S2E**), at comparable levels as WT nTreg cells. The
145 results suggested that an antigen(s) cross-reactive with OVA in NC might activate DO Tconv cells to
146 differentiate into functionally stable pTreg cells, although the number of pTreg cells thus generated was
147 not sufficient to induce OVA-specific oral tolerance (**Fig. 1B** and **1C**). After depletion of these pTreg
148 cells in NC-fed DORF mice by DTx administration **(Fig. S2G** and **S2H)**, EWP feeding efficiently
149 induced pTreg cells, suggesting that the pTreg cells were derived from non-Treg cells upon EWP
150 antigen stimulation, rather than from selective expansion or survival of the pre-existing pTreg cells **(Fig.**
151 **S2I)**.

Taken together, these results indicate that the diet containing cognate antigen drives Tconv cells to differentiate into activated pTreg cells in the intestine, and enables them to acquire Treg-specific epigenetic changes, hence Treg-lineage stability similar to that of nTreg cells. In addition, the quantity of pTreg cells is dependent on the amount of the antigen contained in the diet; thus, more than a certain amount of the antigen is required for generating pTreg cells quantitatively sufficient to establish oral tolerance.

Antigen feeding induces tissue-specific effector-type pTreg cells suppressing effector Tconv cell differentiation.

We next attempted to characterize the dynamics of the differentiation/activation of pTreg and Tconv cells in EWP-fed DORe mice using single-cell RNA-sequencing (scRNA-seq). Analysis of preprocessed 6,449 cells from four hash-tagged and pooled populations of DO^+ $CD4^+$ T cells (i.e., mLN or SI-LP cells in DORe mice NC- or 10% EWP-fed for 4 weeks) identified 13 clusters by the expression of T-lineage signature genes (**Fig. 3A** and **S3A**). EWP feeding resulted in an increase of Cluster 8 (circulating 2), which was *Myb*^{hi} (indicative of augmented T-cell survival and exhaustion) (Yuan et al., 2010; Dias et al., 2017; Tsui et al., 2022), reductions of Cluster 4 (Teff-mix) and 11 (Th1), and conversion of Treg population from Cluster 5 to Cluster 3 in SI-LP (**Fig. 3B**). Compared to Cluster 5, Cluster 3 pTreg cells having increased after EWP feeding highly expressed activation-related genes (*Tnfrsf9*, *Tnfrsf4*, *Tigit,* and *Tnfrsf18*), Th2-type transcription factor (*Gata3*), and tissue repairing-related molecules (*Areg* and *Penk*) (**Fig. 3C**). Supporting these results, gene ontology analysis between Cluster 3 and 5 SI-LP pTreg cells revealed that Cluster 3 pTreg cells expressed a highly activated and proliferative T cell phenotype compared to Cluster 5 pTreg cells (**Fig. 3D**). To analyze further the kinetics of antigen-specific T cells in SI-LP, we re-clustered Cluster 3, 4, 5, and 11 based on commonalities and newly identified 8 clusters (**Fig. 3E-G** and **S3B**). Together with pseudotime analysis (**Fig. 3G**), the analysis suggested that, among $Foxp3^+$ cells (Clusters 0, 1, 4, 6, and 7), Clusters 0 and 7 became activated and differentiated upon EWP stimulation into Cluster 1 and 4, which expressed *Klrg1*, *Areg*, and *Penk*. Among Tconv cells (Clusters 2, 3, and 5), effector T-cell populations with Th1 and Th17 gene signatures appeared to diminish upon EWP feeding (**Fig. 3E**, **3F**, and **S3B**). *Mcl1*, an anti-apoptotic gene, was relatively high in *Sell*$^+$ (i.e., $CD62L^{hi}$) $Foxp3^+$ cells (Cluster 7); *Bcl2* being high in Th1 cells (Cluster 5) (**Fig. S3C**).

We assessed protein expression to validate these findings by comparing EWP- and NC-fed SI-LP pTreg cells (**Fig. 3H-K**). The former showed significantly higher expression of 4-1BB (*Tnfrsf9*), OX40 (*Tnfrsf4*), and TIGIT (*Tigit*), in good correlations with their mRNA expression levels (**Fig. 3H** and **3I**). EWP-fed pTreg cells also contained increased proportions of T-bet$^+$, GATA3$^+$, or RORγt$^+$ pTreg cells compared with NC-fed pTreg cells (**Fig. 3J**). Furthermore, continuous EWP feeding induced Ki-67$^+$ and KLRG1$^+$ pTreg cells (i.e., highly proliferative and differentiated pTreg cells), which were significantly reduced in ratio after cessation of the feeding for 4 weeks (**Fig. 3K**).

We also conducted bulk mRNA-seq to assess the characteristics of pTreg cells in lymphoid and non-lymphoid tissues in EWP-fed mice. pTreg cells in mLNs and skin dLNs possessed more common features compared to those in SI-LP or the ear (**Fig. 3L**), suggesting that pTreg cells generated in the intestine underwent tissue-specific adaptation and acquired a tissue-specific Treg phenotype and function distinct from those of lymph node pTreg cells, as observed in scRNA-seq (**Fig. S3D**) (Miragaia

192 et al., 2019). For example, SI-LP and ear-tissue pTreg cells (corresponding to Clusters 0, 1, 4, 6, and 7
193 in Fig. 3E) were distinct from LN pTreg cells in the expression of apoptosis-related molecules (**Fig.**
194 **S3E**), for example, their lower expression of *Bcl2*, hence being more prone to die by apoptosis after their
195 antigen-specific activation (**Fig. 3M**). Further, among chemokine receptors controlling tissue migration,
196 SI-LP and ear-tissue pTreg cells distinctly expressed CCR9 and CCR5, respectively, in both the mRNA
197 and protein levels (**Fig. 3N, 3O,** and **S3F**).
198 Collectively, these results demonstrate that EWP feeding generates and sustain pTreg cells that
199 can differentiate into tissue-specific effector-type Treg cells that suppress the differentiation/activation
200 of effector Tconv cells.

201 **Specific expression of CD101 by intestinal pTreg cells generated by antigen feeding.**
202 We next searched for specific markers that could differentiate EWP-induced intestinal pTreg cells from
203 other Treg cells, particularly from tTreg cells, by preparing mixed bone marrow chimeric (BMC) mice
204 in which DORe BM-derived pTreg cells and WT (Thy1.1-eFox) mouse BM-derived nTreg cells
205 developed in the same environment (**Fig. 4A**). While NC or 10% EWP feeding for 4 weeks from
206 immediately after bone marrow transfer equally generated WT nTreg cells, only EWP feeding generated
207 DORe BM-derived pTreg cells in mLNs, SI-LP, and SI-IE, and to lesser extents in popliteal LN and
208 spleen, but not in the thymus (**Fig. 4B-4D**). Bulk mRNA-seq of DORe pTreg cells and WT nTreg cells
209 in BMC mice having been EWP-fed for 8 weeks revealed the genes that were differentially expressed
210 between the two Treg populations (**Fig. 4E**). Among such genes normalized for TPM (transcript per
211 million) in the expression level, DORe-pTreg cells showed much higher expression of *Cd101* and *Gpr83*
212 and lower expression of *Icos* when compared with WT nTreg cells from NC- or EWP-fed BMC mice
213 (**Fig. 4F**). Regarding previously reported tTreg markers (Thornton et al., 2010; Weiss et al., 2012),
214 *Ikzf2*(Helios) was low, whereas *Nrp1*(Neuropilin-1) was high, in DORe pTreg cells (**Fig. 4G**).
215 Flowcytometric analysis further confirmed that DORe pTreg cells strongly expressed the CD101 protein
216 in BMC mice (**Fig. 4H**). Similarly, in NC-fed WT (eFox) and DORe mice (**Fig. S2**), ~80% of DORe
217 pTreg cells and ~25% of WT nTreg cells expressed CD101, while Foxp3^{-} Tconv cells scarcely
218 expressed the molecule (**Fig. 4I**).
219 To examine CD101 expression on Foxp3^{+} cells in a more physiological condition, DORe-
220 derived naïve T cells were transferred into WT mice, which were then fed with EWP (**Fig. 5A**).
221 Detectable numbers of DORe pTreg cells were found to be induced in mLN (**Fig. 5B** and **5C**). They
222 highly expressed CD101 and Nrp-1 (**Fig. 5D**).
223 In the thymus of normal mice, CD101 was expressed by a fraction of DN1 (CD4/CD8 double-
224 negative CD44^{+}CD25^{-}) thymocytes, losing its expression along differentiation and again becoming
225 expressed at the CD25^{-}Foxp3^{+}CD4SP Treg precursor stage, with upregulation at mature
226 CD25^{+}Foxp3^{+} Treg cells (**Fig. 5E, 5F**). In the periphery, CD101 expression was limited to Foxp3^{+} T
227 cells, with higher expression by CD44^{+}CD62L^{-} effector Treg cells compared with naïve ones (**Fig. 5G,**
228 **5H**). In addition, CD101 expression by nTreg cells was well correlated with the expression of
229 activation-associated molecules such as Nrp-1, GITR, CD69, CD103, and CD44, especially in mLNs
230 (**Fig. 5I** and **5J**).

231 Taken together, these results indicate that intestinal pTreg cells generated by antigen feeding are
232 distinct from tTreg cells in the expression levels of certain genes, especially CD101.

233 ***In vitro* induction of CD101$^+$ iTreg cells from naïve and antigen-primed Tconv cells by blockade of**
234 **costimulatory signal.**

235 Based on the above results, we investigated how functionally stable iTreg cells similar to CD101$^+$
236 intestinal pTreg cells induced by antigen feeding could be generated *in vitro* from Tconv cells. Previous
237 studies have shown that iTreg cells can be produced *in vitro* by anti-TCR stimulation with plate-bound
238 anti-CD3 mAb in the presence of TGF-β, IL-2, and agonistic anti-CD28 mAb (Zheng et al., 2002; Chen
239 et al., 2003), and that, in the presence of IL-2, iTreg generation was more efficient in the absence of
240 agonistic anti-CD28 mAb (Mikami et al., 2020; Benson et al., 2007). Consistent with this, we found that
241 iTreg cells generated without CD28 signal indeed expressed CD101 at higher levels than those produced
242 with CD28 signal (**Fig. 6A** and **6B**). Moreover, CD28-deficient naïve Tconv cells more efficiently
243 differentiated into iTreg cells with higher expression of CD101 compared with CD28-intact naïve Tconv
244 cells; agonistic anti-CD28 mAb significantly hampered the generation of CD101$^+$ iTreg cells from the
245 latter, but not from the former (**Fig. 6C** and **6D**). Furthermore, TGF-β dose-dependent iTreg induction
246 revealed that TGF-β significantly enhanced CD101 expression in a dose dependent manner only in iTreg
247 cells generated without CD28 signal (**Fig. S4A**).

248 Next, to simulate *in vitro* the condition of intestinal pTreg generation in EWP-fed DORe mice,
249 we examined the effects of CD80/CD86 blockade with CTLA-4-immunoglobulin (CTLA4-Ig) fusion
250 protein on iTreg generation from naïve DORe Tconv cells stimulated with OVA in the presence of
251 splenic DCs (**Fig. S4B**). CTLA4-Ig did not inhibit proliferative differentiation of Foxp3$^+$ cells even at
252 high doses (**Fig. S4C**), increased CD101 expression levels in an IL-2 dependent fashion (**Fig. S4D**), and
253 conferred *Foxp3*-CNS2 hypomethylation on the generated iTreg cells (**Fig. S4E**). With cDC1 and cDC2
254 cells prepared from SI-LP (**Fig. S4F**), CTLA4-Ig in combination with all-trans retinoic acid (ATRA)
255 significantly increased the generation of Foxp3$^+$ cells and enhanced their expression of CD101 on both
256 types of DCs (**Fig. 6E** and **6F**). CTLA4-Ig together with ATRA increased iTreg generation and CD101
257 expression even in the presence of various inflammatory cytokines (**Fig. 6G**). Furthermore, with naïve
258 or effector/memory Tconv cells from dLNs of OVA immunized DORe mice (**Fig. 6H**), CTLA4-Ig
259 effectively augmented iTreg generation and their CD101 expression with naïve Tconv cells and, to
260 lesser degrees, with effector/memory Tconv cells (**Fig. 6I** and **6J**).

261 Taken together, blockade of CD80/CD86 did not hamper iTreg generation with TGF-β, IL-2, and
262 antigen stimulation, rather enhancing the generation of iTreg cells, CD101$^+$ ones in particular. Thus,
263 CD28 signaling is dispensable for iTreg generation, especially in the presence of IL-2. CD101
264 expression could be attributed to the reduction of CD28 co-stimulatory signal in iTreg generation.

265 **Establishment of oral tolerance in antigen-presensitized mice by CD80/CD86 blockade and**
266 **subsequent antigen feeding.**

267 The above result that CTLA4-Ig enabled iTreg cell induction from antigen-primed Tconv cells prompted
268 us to determine whether *in vivo* CTLA4-Ig treatment would be able to establish oral tolerance even in
269 precedingly antigen-primed mice (**Fig. 7A**). When DORe mice were OVA sensitized at the right ear,

injected intraperitoneally (i.p.) with CTLA4-Ig at various doses or saline, and then fed with EWP chow for 4 days, the right ear swelling gradually subsided during the feeding whether the mice were treated with CTLA4-Ig or not (**Fig. S5A**). However, mice treated with saline or low-dose (2 μg) CTLA4-Ig showed significant weight loss during EWP feeding (**Fig. S5B**), contrasting with no weight loss in the mice CTLA4-Ig-treated at high (10 or 50 μg) doses. The weight loss recovered after cessation of the feeding (**Fig. 7B**). When these mice were OVA challenged to the left ear after 4-day EWP feeding, those treated with high dose (10 or 50 μg) CTLA4-Ig did not show ear swelling or succumb to histologically evident inflammation, contrasting with other groups suffering from severe ear swelling and dermatitis (**Fig. 7C** and **S5C**). Notably, contrasting with the CTLA4-Ig/EWP-treated mice exhibiting no ear swelling, the CTLA4-Ig/NC-treated mice developed severe ear swelling and dermatitis. The prevention of ear swelling was also observed with the higher antigen dose (30% EWP-containing chow), while the lower antigen dose (1% EWP) displayed a reduced preventive effect (**Fig. S5D-F**). These results taken together indicated that both CTLA4-Ig treatment and antigen feeding were required for inducing the unresponsiveness.

There were little differences among these mouse groups in the ratio of Foxp3 cells on day 15 and 33, with a tendency of Treg increase in the CTLA4-Ig-treated mice (**Fig. 7D** and **7E**). The ratios of cytokine-secreting cells among DO Tconv cells were not significantly different among the mouse groups at day 15, except significant reduction of the ratio of IL-17$^+$ cells in dLNs of the CTLA4-Ig-treated groups compared with the saline-treated or NC-fed mice (**Fig. 7F**). IFN-γ$^+$ cells as well as IL-17$^+$ cells in the former were significantly lower compared with the latter at day 33 (**Fig. 7G**). The results suggested that the high ratios of Foxp3$^+$ cells in low-dose CTLA4-Ig- or saline-treated group could be attributed to their secondary expansion due to inflammation.

The pTreg cells having developed in EWP-fed mice, whether treated with CTLA4-Ig or saline, showed Treg-specific DNA demethylation at the *Foxp3* CNS2 region, suggesting their functional stability as Treg cells (**Fig. S5G**). In contrast to no significant differences in total Foxp3$^+$ cells in the ear or dLNs (**Fig. 7D** and **7E**), CD101 expression by Foxp3$^+$ cells was significantly upregulated and the ratio of CD101$^+$Foxp3$^+$ cells increased at day 15 in the right ear and its dLNs of the CTLA4-Ig-treated mice depending on the dose of CTLA4-Ig, similarly in the left ear and its dLNs at day 33 (**Fig. 7H** and **7I**). Depletion of Foxp3$^+$ cells by DTx administration on day 15 and 18 in CTLA4-Ig-treated and then EWP-fed DORF mice resulted in an exacerbated ear inflammation, a decrease in pTreg cells in the inflamed ear tissue, and an increase in IL-4$^+$ T cells in dLNs (**Fig. 7J, S5H,** and **S5I**). CD101$^+$ Foxp3$^+$ cells were also significantly decreased in the inflamed ear tissue, dLNs and mLNs (**Fig. 7K**).

These results collectively demonstrate that CD80/CD86 blockade by CTLA4-Ig and subsequent antigen feeding is able to establish oral tolerance in antigen-presensitized mice through inducing CD101$^+$ pTreg cells.

Discussion

It has been controversial whether pTreg cells are as functionally stable as tTreg cells and how they can be functionally and phenotypically distinguished from the latter. We have shown here that intestinal pTreg cells induced by antigen feeding are similar to tTreg cells. They not only express Foxp3 but also possess Treg-type epigenetic changes such as DNA hypomethylation at the Treg-specific demethylation

310 regions and activation of the Treg-specific super-enhancers at Treg signature gene loci including *Foxp3*,
311 *Il2ra*, and *Ctla4*. Additionally, these cells are Helios^{hi} and Neuropilin-1^{hi} as are tTreg cells (Thornton et
312 al., 2010; Weiss et al., 2012), while pTreg cells newly generated in BMC mice by EWP feeding were
313 Helios^{low}. It is likely that chronic stimulation may gradually upregulate Helios and Neuropirin-1 in
314 pTreg cells (Szurek et al., 2015; Thornton and Shevach, 2019). In addition, the generated pTreg cells are
315 in a tissue-adapted state as seen with tissue-specific and -resident tTreg cells (Muñoz-Rojas and Mathis,
316 2021; Dikiy and Rudensky, 2023), as illustrated by the expression of *Tnfrsf9*, *Tnfrsf4*, *Gata3*, and *Areg*
317 as well as skin-specific chemokine receptors such as *Ccr5* and *Ccr8* (Schiering et al., 2014; Miragaia et
318 al., 2019). However, despite these immunological properties indicative of functional competence and
319 stability of pTreg cells induced by antigen feeding, cessation of antigen administration resulted in
320 decline of oral tolerance with diminution of proliferative and Bcl-2^{+} (i.e., apoptosis resistant) pTreg cells.
321 This could be, at least in part, attributed to the antigen specificity of the induced pTreg cells, as well as
322 the strength and duration of antigen stimulation delivered to them in the periphery. tTreg cells are more
323 self-reactive than Tconv cells, hence tonically stimulated in the periphery for better survival (Hsieh et al.,
324 2004, 2012). In contrast, pTreg cells once generated by antigen feeding may require persistent or
325 frequent stimulation by the administered cognate non-self antigen for their survival to maintain tolerance,
326 despite their possession of Treg-specific epigenetic alterations and acquisition of tTreg-like
327 immunological properties.

328 The generation of intestinal pTreg cells by antigen feeding depends on the quantity of cognate
329 antigen contained in the diet. Notably, even DORe mice fed with NC or Ag-free diet developed Foxp3^{+}
330 T cells particularly in SI-LP and LI-LP, and that they are phenotypically and epigenetically
331 indistinguishable from pTreg cells generated by EWP-high diet. In NC-fed mice, a certain diet protein(s)
332 or a microbial substance(s) cross-reactive with OVA could likely stimulate DO Tconv cells to
333 differentiate into pTreg cells. The NC-induced pTreg cells were, however, smaller in number and less
334 activated (e.g., lower in CD25 expression) than the high-EWP-induced pTreg cells and unable to
335 suppress ear swelling upon antigen exposure. These findings indicate that induction of oral tolerance
336 depends on the number of antigen-specific pTreg cells and/or their activation status, and that both events
337 depend on the quantity of the ingested antigen. This dependency of oral tolerance on the quantity of
338 administered antigen may also be the case in establishing mucosal tolerance via other routes, for
339 example, by sublingual antigen administration for allergy treatment (Windom et al., 2024).

340 Intestinal pTreg cells induced by antigen feeding specifically express CD101, which is also
341 highly specific for iTreg cells generated *in vitro* by the absence or blockade of CD28 co-stimulatory
342 signal. Intestinal pTreg cells found in NC-fed mice, as discussed above, similarly expressed CD101,
343 whereas nTreg cells in mLNs in WT mice hardly expressed the molecule even after high-EWP feeding.
344 Furthermore, *in vivo* treatment with CTLA4-Ig for oral tolerance induction generated CD101^{+} pTreg
345 cells in the antigen-challenged tissue, and the degree of expression depended on the dose of CTLA4-Ig.
346 Recent studies have shown that CD101 is highly expressed by tissue-resident Treg cells compared to
347 circulating ones (Kaminski et al., 2023); its expression is correlated with the level of FOXP3 expression
348 in human Treg cells (Ferraro et al., 2014), and with *in vivo* Treg suppressive capacity on GvHD and IBD
349 in mouse models (Fernandez et al., 2007; Schey et al., 2016). Furthermore, a genetic variant of CD101

350 contributes to genetic susceptibility to type 1 diabetes in an animal model through affecting Treg and
351 other immune cells (Rainbow et al., 2011; Mattner et al., 2019). CD101 is reportedly expressed by
352 exhausted $CD8^+$ T cells as well (Hudson et al., 2019). These findings and ours, when taken together,
353 suggest that CD101 plays a role in modulating TCR and CD28 signaling (Soares et al., 1998), especially
354 the latter, for pTreg development in the intestine and iTreg generation from Tconv cells *in vitro*. The
355 molecular basis of the function of CD101 and its ligand, which is currently unknown, remains to be
356 determined. Nevertheless, CD101 could be a useful marker for pTreg cells, especially those induced by
357 $CD80/CD86^{low}$ tolerogenic DCs, which transduce TCR signal with reduced CD28 signal.

358 CD80/CD86 blockade by CTLA4-Ig facilitates *in vivo* $CD101^+$ pTreg induction and *in vitro*
359 $CD101^+$ iTreg generation. The blockade and antigen stimulation allow both Treg populations to
360 proliferate and enable them to acquire the Treg-type epigenome, hence their functional and cell-lineage
361 stability (Mikami et al., 2020). IL-2 is essential for this Treg generation because it can compensate for
362 the absence or reduction of CD28 signaling, hampering anergy induction and enabling more efficient
363 generation of iTreg cells than without the blockade. It is plausible that *in vivo* provision of IL-2 could
364 further facilitate pTreg cell generation by antigen feeding after CD80/CD86 blockade. In addition, APCs,
365 especially DCs, play key roles in pTreg cell induction by antigen feeding (Esterházy et al., 2016; Brown
366 and Rudensky, 2023). Both cDC1 and cDC2 were able to generate iTreg cells *in vitro* under
367 CD80/CD86 blockade. In addition to the role of CD80/CD86 for Treg induction by APCs, it has been
368 shown that $PD\text{-}L1^+$ DCs are potent in inducing antigen-specific Treg cells and that PD-L1 blockade
369 inhibits the induction (Wang et al., 2008; Francisco et al., 2009). We and others have shown that Treg
370 cells are able to inhibit the T-cell stimulatory activity of APCs by reducing their CD80/CD86 expression
371 via trogocytosis and transendocytosis, which are dependent on Treg-expressed CTLA-4 (Wing et al.,
372 2008; Onishi et al., 2008; Qureshi et al., 2011; Tekguc et al., 2021). This CD80/CD86 reduction on
373 APCs results in dissociation of PD-L1 from *cis*-bound CD80, increasing free-PD-L1 available for the
374 inhibition of PD-1 expressing effector T cells (Tekguc et al., 2021). CTLA4-Ig can have a similar effect
375 by disrupting *cis*-CD80-PD-L1 interaction depending on the ratio of CD80 to PD-L1 on APCs (Tekguc
376 et al., 2021; Oxley et al., 2024; Robinson et al., 2024). We have shown in this report that reduction or
377 abrogation of CD28 signal alone (for example, by utilizing CD28-deficient naïve Tconv cells), without
378 modulating PD-L1/PD-1 interaction, suffices to generate iTreg cells effectively. It still needs to be
379 determined, however, whether enhanced signaling from free-PD-L1 on APCs to $PD\text{-}1^+$ Tconv cells
380 facilitates the conversion of the latter to pTreg cells.

381 Prior antigen sensitization and the following antigen feeding evoked systemic inflammation.
382 CTLA4-Ig treatment before antigen feeding not only prevented the systemic inflammation but also
383 suppressed local inflammation at the site of antigen exposure. These findings carry some clinical
384 implications. First, it is conceivable that certain food allergies might be a consequence of prior antigen
385 sensitization at other sites of the body, as proposed as the dual-allergen-exposure hypothesis for food
386 allergy (Lack, 2008). Second, CTLA4-Ig has been used for treatment of allergy on the assumption that it
387 may suppress effector T-cell activation and IgE production (Van Wijk et al., 2005). We have shown here
388 that CTLA4-Ig can additionally facilitate the generation of antigen-specific functionally stable pTreg
389 cells from antigen-primed Tconv cells when combined with subsequent antigen feeding. Third, this

390 approach to establishing oral tolerance by CD80/CD86 blockade and antigen feeding can be useful for
391 mucosal tolerance induced by other ways, for example, by sublingual or subcutaneous antigen treatment
392 to treat chronic allergy. It could also be extended to the induction of immune tolerance towards
393 microbial antigens derived from intestinal commensal bacteria to treat inflammatory bowel disease.
394 In conclusion, antigen-specific functionally stable CD101$^+$ pTreg cells are generated in the
395 intestine by antigen feeding and engaged in the establishment of long-term systemic antigen-specific
396 immune tolerance. CD101$^+$ iTreg cells with similar phenotype and function can also be produced *in*
397 *vitro* from antigen-specific Tconv cells by depriving CD28 costimulation during their induction,
398 suggesting a common developmental basis for these pTreg and iTreg cells. Furthermore, continuous
399 antigen feeding combined with CD28 co-stimulation blockade is able to generate CD101$^+$ pTreg cells
400 and establish immune tolerance even in previously antigen-sensitized animals.

401 **Materials and methods**

402 **Mice**

403 BALB/c mice were purchased from SLC or CLEA. DO11.10 TCR transgenic mice, *Rag2*-deficient mice,
404 Foxp3-eGFP (eFox) reporter mice, Thy1.1-eFox mice, Foxp3-DTR-GFP mice, and *CD28*-deficient mice
405 were previously described (Mikami et al., 2020; Kim et al., 2007; Shahinian et al., 1993). All mice were
406 maintained under specific pathogen-free conditions. All procedures were conducted in accordance with
407 the National Institutes of Health Guide for the Care and Use of Laboratory Animals and approved by the
408 Committee on Animal Research of Osaka University.

409 **Food modification**

410 AIN-93G diet and egg-white-powder (EWP)-added food were purchased from CLEA. AIN-93G diet
411 was used as antigen-free food (**Table. 1**). CE-2 (CLEA) as normal chow (NC) was used as standard food
412 in the animal facility. For DORe mice, food modification began at 2 weeks of age under milk feeding or
413 at 4 weeks of age after weaning, and continued until 8 weeks of age. For bone marrow chimeric mice,
414 the food modification was started at the time of bone marrow cell transfer, and continued for 4-8 weeks.

415 **Epicutaneous sensitization of OVA antigen to mice**

416 The procedure was described in previous studies (Shimura et al., 2016). Mice were anesthetized with
417 isoflurane. Both ears were treated with tape stripping five or six times using surgical tape (21N,
418 Nichiban, Tokyo, Japan). Then, a total of 12.5 µl of 10 mg/ml of papain with 10 mg/ml OVA was
419 applied to each side of the surface of mouse ear. This treatment was repeated twice per week for 2 weeks.
420 During the experimental period, ear thickness was measured daily using a digital caliper. For depleting
421 Foxp3$^+$ cells in the experiment, diphtheria toxin (400 ng in 200 µl PBS) was injected intraperitoneally
422 twice per week into the Foxp3-DTR-GFP background mice.

423 **Histopathology**

424 Tissues were fixed with 10% formalin, embedded in paraffin blocks, and sectioned and stained by
425 hematoxylin and eosin. For ear swelling test, histological and pathological scoring was performed by
426 following criteria and summed up; disorder of epidermis: 1-3, disorder of dermis: 1-3, disorder of
427 hypodermis: 1-3, cell invasion: 1-3, and range of inflammation: 1-3.

428 **Isolation of ear-infiltrating immune cells**

429 Dissected ears were minced into small pieces with scissors and digested in the isolation buffer (HBSS(−)
430 with 2% FBS, 2 mg/ml Collagenase D (Roche), and 20 µg/ml DNaseI (Roche)) with 1,300 rpm shaking
431 at 37°C for 2 h. The suspension was then passed through a 70-µm mesh and mash the debris by using a
432 syringe plunger. The flow-through was centrifuged at 500xg at 4°C for 5 min. The pellet was washed
433 and resuspended with FACS buffer. Isolated cells were used for flowcytometry directly or first
434 stimulated with PMA and ionomycin in the presence of GolgiStop (BD) for 4 h at 37°C for subsequent
435 intracellular cytokine staining.

436 **Isolation of lymphocytes from intestinal mucosa**

437 Intestines were harvested from mice, the lumen was opened longitudinally with scissors, the luminal
438 contents were removed, and the tissues were washed with FACS buffer. After cutting the tissues into 2
439 cm, they were incubated with IE isolation buffer (HBSS(−) with 2% fetal bovine serum (FBS), 1 mM
440 EDTA (Nacalai)) at 37°C for 30 min. The tissues were then incubated with LP isolation buffer
441 (HBSS(−) with 2% FBS, 1 mg/ml collagenase D (Roche), and 10 µg/ml DNaseI (Roche)) at 37°C for 30
442 minutes. The suspension was then passed through a 70-µm mesh, and the debris was mashed using a
443 syringe plunger. The flow-through was centrifuged at 500xg at 4°C for 5 min. The pellet was
444 resuspended with 40% Percoll solution, then layered with 80% Percoll solution and centrifuged at 2,000
445 rpm at room temperature for 20 min without acceleration and brake. The interface was collected and
446 washed with FACS buffer.

447 **Generation of mixed bone marrow chimeric mice**

448 Bone marrow cells were harvested from the femur and tibia of mice, using a 23G needle and syringe.
449 After lysing red blood cells, $CD3e^{+}$ T cells were removed using the MACS negative selection system
450 (Miltenyi Biotec) or the BD IMag Cell Separation System (BD) following the manufacturer's protocol.
451 T cell-depleted bone marrow cells from Thy1.1-eFox and DORe mice were mixed at a ratio of 1:2 in
452 PBS buffer and injected intravenously into $CD45.1^{+}$ *Rag2*-deficient mice as recipientsthat had been
453 irradiated at 4.0 Gy. After 4 weeks or more later from bone marrow reconstitution, chimeric mice were
454 sacrificed and analyzed.

455 **Cell preparation, cell sorting, and flowcytometry**

456 For the preparation of DORe-pTreg cells, $CD4^{+}DO11.10^{+}CD25^{+}$Foxp3-$eGFP^{+}$ cells were sorted from
457 the peripheral lymph nodes and peripheral tissues harvested from DORe mice. Peripheral Tconv cells
458 were defined as these gating below; naïve Tconv cells ($CD4^{+}CD25^{-}$Foxp3-$eGFP^{-}CD62L^{hi}CD44^{lo}$) and
459 effector Tconv cells ($CD4^{+}CD25^{-}$Foxp3-$eGFP^{-}CD62L^{lo}CD44^{hi}$). As antigen presenting cells, cDC1
460 ($CD45^{+}CD11c^{+}$IA-$IE^{+}CD103^{+}CD11b^{-}$) and cDC2 ($CD45^{+}CD11c^{+}$IA-$IE^{+}CD103^{+}CD11b^{+}$) fractions
461 were sorted from SI-LP in CD45.1 WT mice. BD Cytofix/Cytoperm Fixation/Permeabilization Kit (BD)
462 was used for intracellular staining for cytokines used following stimulation with PMA and Ionomycin
463 and treatment with Golgi-Stop (BD Biosciences), and the Foxp3 staining kit (eBiosciences) was used for
464 transcriptional factors or intracellular molecules. Flowcytometry analysis and cell sorting were
465 performed using FACSCantoII, FACSCellesta, FACSAriaII, and FACSAriaFusion (BD Biosciences).
466 Antibodies used in this study are listed (**Table S2**).

467 **CpG methylation analysis by bisulfite sequencing in Treg-specific demethylation regions**
468 Bisulfite sequencing analysis was performed as previously described (Arai et al., 2022). Briefly, cells
469 were sorted by FACSAriaII, and gDNA was extracted by phenol extraction followed by ethanol
470 precipitation. Bisulfite base conversion was carried out using the Methyl Easy Xceed Rapid DNA
471 Bisulphite Modification Kit (Human Genetic Signatures) or following our original methods previously
472 described. PCR primer sequences for Treg-specific demethylated regions are available (Ohkura et al.,
473 2012; Arai et al., 2022).

474 **ChIP-seq**
475 ChIP-seq experiments were performed as previously described (Kitagawa et al., 2017; Kawakami et al.,
476 2021). Briefly, sorted cells were fixed with 1% formaldehyde (ThermoScientific) for 10 min for anti-
477 histone ChIP at room temperature. After nuclear extraction, chromatin lysate was fragmentated using
478 Picoruptor (Diagenode), 30 sec sonication and 30 sec cooling for 7 cycles at 4℃, before
479 immunoprecipitation. Immunoprecipitated chromatin lysate was reverse cross-linked at 65℃ for 24 h,
480 followed by purification and library preparation using NGS Library Preparation kit for IonS5
481 (ThermoScientific) or NEBNext Ultra II DNA Library Prep Kit for Illumina (Illumina) according to the
482 manufacturer's instructions. Raw data were generated using the IonS5 sequencing system
483 (ThermoScientific) or NextSeq500 (Illumina).

484 **ATAC-seq**
485 ATAC-seq was performed as previously described (Corces et al., 2017). Briefly, sorted cells (up to
486 100,000 cells) were lysed with100 µl of lysis buffer (0.01% digitonin, 0.1% NP-40, 0.1% Tween 20 in
487 resuspension buffer; 10 mM Tris-HCl pH7.5, 100 mM NaCl, 3 mM $MgCl_2$) for 3 min on ice. After
488 removal of lysis buffer by centrifugation, Tn5 tagmentation was performed using Illumina Tagment
489 DNA TDE1 Enzyme and Buffer Kits (Illumina) at 37℃ for 30 min, with shaking at 1,000 rpm. After
490 purification using DNA Clean & Concentrator-5 (Zymo Research), tagmented DNA was amplified
491 using NEBNext High-Fidelity PCR Master Mix (New England BioLabs) with the following prepared
492 DNA libraries were purified using DNA Clean & Concentrator-5 or Ampure XP (Beckman Coulter).
493 Sequencing was performed using NextSeq500 or NovaSeq (Illumina).

494 **Data processing and analyses of ChIP-seq and ATAC-seq data**
495 For ChIP-seq analysis, raw sequence reads were inspected and trimmed using Trim-galore (v0.6.6)
496 (Babraham Bioinformatics). Trimmed reads were mapped to mm10 genome using Bowtie2 (v2.3.5)
497 (Langmead and Salzberg, 2012) with the following options; --local --very-sensitive-local. Mapped reads
498 were sorted using Samtools (v1.6)(Li et al., 2009), then converted into bigwig files for visualization by
499 bamCoverage (v3.1.3), included deepTools package(Ramírez et al., 2016), with the following options; -
500 of bigwig --binSize 5 -p max --normalizeUsing CPM --smoothLength 15 –ignoreDuplicates. Peak
501 calling was performed using MACS2 (v2.1.1.20160309)(Feng et al., 2012) with the following options;
502 macs2 callpeak -t ${filename} -name ${outputfilename} -f BAM -g mm --SPMR --nolambda --nomodel
503 --bdg --call-summits. For defining Treg or Tconv-specific enhancer regions, narrowPeak files were
504 concatenated, sorted. Sorted narrowPeak file was merged using bedtools (v2.30.0)(Quinlan and Hall,
505 2010) and then converted into SAF format file. SAF peak file was annotated using HOMER

506 (v4.11)(Heinz et al., 2010). Count files were generated using featureCounts(Liao et al., 2014) with the
507 following options; -a annotated.saf -F SAF -p -o counts.txt ${BAM}. Differential expression analysis
508 was performed using DESeq2. To assess the tag density of H3K27ac signals in Treg and naïve Tconv
509 cells, matrix files were created using computeMatrix (v3.1.3), included deepTools package, with the
510 following options; --beforeRegionStartLength 2000 --regionBodyLength 5000 --afterRegionStartLength
511 2000 --skipZeros, then visualized plotProfile command.
512 For ATAC-seq analysis, sequence reads were mapped to mm10 genome using Bowtie2 (v2.3.5)
513 by following options; --very-sensitive. Mapped reads were sorted by Samtools (v1.9) and then converted
514 into bigwig files for visualization by bamCoverage (v3.1.3) with the following options; -of bigwig --
515 binSize 5 -p max --normalizeUsing CPM --smoothLength 15 –ignoreDuplicates. Peak calling was
516 performed using MACS2 (v2.1.1.20160309) with the following options; macs2 callpeak -t ${filename} -
517 name ${outputfilename} -f BAM -g mm --SPMR --nolambda --nomodel --shift -75 --extsize 150 --keep-
518 dup all --bdg --call-summits.
519 IGV Integrated genome viewer was used to visualize peak or region data.

520 **Single-cell RNA-seq and analysis**

521 Single-cell RNA-Seq was performed on a Chromium instrument (10X Genomics) following the user
522 guide manual for 30 v3 or 50 v2 chemistry. Briefly, FACS-sorted DORe-derived T cells isolated from
523 mLNs and SI-LP were stained with TotalSeq anti-mouse Hashtag Antibody (BioLegend), and washed
524 three times with FACS buffer. Cells were resuspended with FACS buffer to a final concentration of
525 approximately 1,000 cells/µl with a viability above 90%. Capturing cells in droplets, reverse
526 transcription, and cell barcoding were performed on the Chromium Controller (10x Genomics), followed
527 by PCR amplification and library construction using Chromium Next GEM Single Cell 5' Kit v2. Final
528 libraries were sequenced on NovaSeq6000 (Illumina), 20,000 reads/cell for mRNA and 5,000 reads/cell
529 for antibody-derived tags.
530 Sequenced reads were quantified using Cell Ranger (v5.0.0) with the pre-built reference refdata-
531 gex-mm10-2020-A downloaded from 10x Genomics' website. Quantified expressions were
532 preprocessed and visualized using Seurat (v4.1.3 or v5.0.1)(Hao et al., 2021). Differentially expressed
533 genes were calculated using "FindMarkers" function based on the non-parametric Wilcoxon rank sum
534 test in Seurat. Gene ontology analysis was performed using clusterProfiler (v4.10.0)(Wu et al., 2021).
535 For the trajectory analysis, selected cells were re-clustered and ordered using Monocle3 (v1.3.4)(Cao et
536 al., 2019).

537 **Bulk RNA-seq and analysis**

538 Bulk RNA-seq was performed as below. Briefly, FACS-sorted cells were lysed by RLT RNA lysis
539 buffer (Qiagen) containing 2-mercaptoethanol to a final concentration of approximately 1,000 cells/10
540 µl followed by reverse transcription using the SMART-seq v4 Ultra Low Input RNA Kit for Sequencing
541 (Clontech). Library preparation was performed using the Kapa Library preparation kit for IonTorrent or
542 for Illumina (KAPA) by following the manufacturer's protocol. Sequencing of cDNA libraries was
543 performed on IonS5 (Thermo Scientific), NextSeq500, or NovaSeq6000 (Illumina).

544 Sequenced reads were inspected and trimmed using Trim-galore (v0.6.6) and aligned to the
545 mouse genome GRCm38/mm10 using STAR (v2.7.7a)(Dobin et al., 2013). Reads counts at the gene
546 level were calculated using RSEM (v1.3.1)(Li and Dewey, 2011). Normalization for library size and
547 differential expression analysis were performed using DESeq2 (v1.32.0)(Love et al., 2014).

548 **Cell culture**

549 Cell culture was performed in RPMI 1640 supplemented with 10%(v/v) FBS, 60 g/ml penicillin G, 100
550 g/ml streptomycin, and 0.1 mM 2-mercaptoethanol. For in vitro Treg induction, sorted naïve Tconv cells
551 were stimulated with plate-bound anti-CD3e mAb (clone: 145-2C11) and soluble anti-CD28 mAb
552 (clone: 37.51) in the presence of 100 U/ml hIL-2 (Shionogi) and 5 ng/ml rhTGF-β_1 (R&D Systems). For
553 the co-culture experiment, DORe-derived naïve or effector/memory Tconv cells were stimulated by
554 sorted APCs, 5 μM $OVA_{323-339}$ peptide (MBL Co., LTD., MedChemExpress), 100 U/ml rhIL-2, and 2.5
555 ng/ml rhTGF-β_1 and with or without 10 nM ATRA supplementation (Wako) or 10 μg/ml CTLA4-Ig
556 (abatacept; Orencia, BMS) for 72 hours.

557 **Statistics**

558 Values were expressed as mean ± SEM. Statistical significance was assessed by Student's *t* test or
559 Welch's *t* test (two groups) following *F* test. One-way ANOVA and Tukey's HSD or Tukey-Kramer test
560 were conducted for multiple comparisons. A p-value < 0.05 was considered statistically significant, and
561 every p value was shown in the figures.

562 **Online supplemental materials**

563 Fig. S1 shows pTreg generation and maintenance by antigen feeding. Fig. S2 shows the development of
564 pTreg cells in NC-fed DORe mice. Fig. S3 shows single-cell RNA-seq analysis of T cells in DORe mice
565 and bulk mRNA-seq analysis of pTreg cells from different tissues after EWP feeding. Fig. S4 shows
566 dose effects of CTLA-4-Ig, TGF-β, and IL-2 on iTreg generation and the gating strategy for isolating
567 intestinal DCs. Fig. S5 shows the effects of CD80/CD86 blockade and subsequent antigen feeding on
568 antigen-presensitized mice. Table S1 indicates nutritional facts of modified foods. Table S2 lists the
569 antibodies used in the study.

570 **Data availability**

571 The raw data (fastq files) from ATAC-seq, ChIP-seq, RNA-seq, and scRNA-seq experiments have been
572 deposited in the DDBJ BioProject database, with links to BioProject accession number PRJDB18773.
573 All data needed to evaluate the conclusions are present in the paper or the Supplementary Materials.

574 **Acknowledgments**

575 We thank all Sakaguchi lab members, particularly: R. Ishii and M. Matsuura for their technical
576 assistance, C. Tay and S.K. Singh for critical reading of the manuscript. We would like to thank K.
577 Kawade for advising us about the production of modified foods. The genomic sequencing and
578 bioinformatic analysis were conducted using the facility at the Genome Information Research Center of
579 the Research Institute for Microbial Diseases, Osaka University.

580 Funding: This study was supported by the Japan Society for the Promotion of Science (JSPS)
581 grant-in-aid for JSPS Fellows (20J20443 to M.A.), JSPS Grant-in-Aid for Early-Career Scientists

582 (20K16279 to R.K.), JSPS Grant-in-Aid for Scientific Research (23H02733 to R.K.), INFRONT Office
583 of Director's Research Grants Program (to R.K.), Grant from Nipponham Foundation for the Future of
584 Food (to R.K.), JSPS Grant-in-Aid for Specially Promoted Research (16H06295 to S.S.), JSPS Grant-in-
585 Aid for Scientific Research (24H00610 to S.S.), and Leading Advanced Projects for Medical Innovation
586 (LEAP; 18gm0010005 to S.S.).

587 Author contributions: M.A. initiated the study. M.A, R.K., N.M., and S.S. designed experiments.
588 M.A., R.K., A.S., and T.K. performed food modification experiment. M.A., Yo.N., and D.M. performed
589 scRNA-seq experiment. M.A. and Ya.N. performed library preparation with advice from N.O. M.A.
590 analyzed all data. M.A. and S.S. wrote the manuscript.

591 Disclosure: The authors declare that they have no conflict of interest associated with this manuscript.

592 **References**

593 Arai, M., A. Fukuda, R. Morimoto, Y. Nakamura, Z. Ci, and S. Sakaguchi. 2022. Protocol to evaluate
594 cell lineage stability of mouse natural and induced regulatory T cells using bisulfite sequencing.
595 *STAR Protocols*. 3:101694. doi:10.1016/j.xpro.2022.101694.

596 Benson, M.J., K. Pino-Lagos, M. Rosemblatt, and R.J. Noelle. 2007. All-trans retinoic acid mediates
597 enhanced T reg cell growth, differentiation, and gut homing in the face of high levels of co-
598 stimulation. *The Journal of Experimental Medicine*. 204:1765–1774. doi:10.1084/jem.20070719.

599 Brown, C.C., and A.Y. Rudensky. 2023. Spatiotemporal regulation of peripheral T cell tolerance.
600 *Science*. 380:472–478. doi:doi: 10.1126/science.adg6425.

601 Cao, J., M. Spielmann, X. Qiu, X. Huang, D.M. Ibrahim, A.J. Hill, F. Zhang, S. Mundlos, L.
602 Christiansen, F.J. Steemers, C. Trapnell, and J. Shendure. 2019. The single-cell transcriptional
603 landscape of mammalian organogenesis. *Nature*. 566:496–502. doi:10.1038/s41586-019-0969-x.

604 Cerovic, V., O. Pabst, and A.M. Mowat. 2024. The renaissance of oral tolerance: merging tradition and
605 new insights. *Nat Rev Immunol*. doi:10.1038/s41577-024-01077-7.

606 Chase, M.W. 1946. Inhibition of Experimental Drug Allergy by Prior Feeding of the Sensitizing Agent.
607 *Experimental Biology and Medicine*. 61:257–259. doi:10.3181/00379727-61-15294P.

608 Chen, W., W. Jin, N. Hardegen, K. Lei, L. Li, N. Marinos, G. McGrady, and S.M. Wahl. 2003.
609 Conversion of Peripheral CD4+CD25− Naive T Cells to CD4+CD25+ Regulatory T Cells by TGF-
610 β Induction of Transcription Factor *Foxp3*. *The Journal of Experimental Medicine*. 198:1875–1886.
611 doi:10.1084/jem.20030152.

612 Coombes, J.L., K.R.R. Siddiqui, C.V. Arancibia-Cárcamo, J. Hall, C.-M. Sun, Y. Belkaid, and F. Powrie.
613 2007. A functionally specialized population of mucosal CD103+ DCs induces Foxp3+ regulatory T
614 cells via a TGF-β– and retinoic acid–dependent mechanism. *The Journal of Experimental Medicine*.
615 204:1757–1764. doi:10.1084/jem.20070590.

616 Corces, M.R., A.E. Trevino, E.G. Hamilton, P.G. Greenside, N.A. Sinnott-Armstrong, S. Vesuna, A.T.
617 Satpathy, A.J. Rubin, K.S. Montine, B. Wu, A. Kathiria, S.W. Cho, M.R. Mumbach, A.C. Carter,
618 M. Kasowski, L.A. Orloff, V.I. Risca, A. Kundaje, P.A. Khavari, T.J. Montine, W.J. Greenleaf, and
619 H.Y. Chang. 2017. An improved ATAC-seq protocol reduces background and enables interrogation
620 of frozen tissues. *Nature Methods*. 14:959–962. doi:10.1038/nmeth.4396.

621 Dias, S., A. D'Amico, E. Cretney, Y. Liao, J. Tellier, C. Bruggeman, F.F. Almeida, J. Leahy, G.T. Belz,
622 G.K. Smyth, W. Shi, and S.L. Nutt. 2017. Effector Regulatory T Cell Differentiation and Immune
623 Homeostasis Depend on the Transcription Factor Myb. *Immunity*. 46:78–91.
624 doi:10.1016/j.immuni.2016.12.017.

625 Dikiy, S., J. Li, L. Bai, M. Jiang, L. Janke, X. Zong, X. Hao, B. Hoyos, Z.-M. Wang, B. Xu, Y. Fan,
626 A.Y. Rudensky, and Y. Feng. 2021. A distal Foxp3 enhancer enables interleukin-2 dependent
627 thymic Treg cell lineage commitment for robust immune tolerance. *Immunity*. 54:931–946.

628 Dikiy, S., and A.Y. Rudensky. 2023. Principles of regulatory T cell function. *Immunity*. 56:240–255.
629 doi:10.1016/j.immuni.2023.01.004.

630 Dobin, A., C.A. Davis, F. Schlesinger, J. Drenkow, C. Zaleski, S. Jha, P. Batut, M. Chaisson, and T.R.
631 Gingeras. 2013. STAR: Ultrafast universal RNA-seq aligner. *Bioinformatics*. 29:15–21.
632 doi:10.1093/bioinformatics/bts635.

633 Du Toit, G., M.F. Huffaker, S. Radulovic, M. Feeney, H.R. Fisher, M. Byron, L. Dunaway, A. Calatroni,
634 M. Johnson, R.-X. Foong, A. Marques-Mejias, I. Bartha, M. Basting, H.A. Brough, C. Baloh, T.M.

635 Laidlaw, H.T. Bahnson, G. Roberts, M. Plaut, L.M. Wheatley, G. Lack, and for the Immune
636 Tolerance Network LEAP-Trio Trial Team. 2024. Follow-up to Adolescence after Early Peanut
637 Introduction for Allergy Prevention. *NEJM Evidence*. 3. doi:10.1056/EVIDoa2300311.

638 Du Toit, G., G. Roberts, P.H. Sayre, H.T. Bahnson, S. Radulovic, A.F. Santos, H.A. Brough, D.
639 Phippard, M. Basting, M. Feeney, V. Turcanu, M.L. Sever, M. Gomez Lorenzo, M. Plaut, and G.
640 Lack. 2015. Randomized Trial of Peanut Consumption in Infants at Risk for Peanut Allergy. *N*
641 *Engl J Med*. 372:803–813. doi:10.1056/NEJMoa1414850.

642 Esterházy, D., J. Loschko, M. London, V. Jove, T.Y. Oliveira, and D. Mucida. 2016. Classical dendritic
643 cells are required for dietary antigen–mediated induction of peripheral Treg cells and tolerance. *Nat*
644 *Immunol*. 17:545–555. doi:10.1038/ni.3408.

645 Faria, A.M.C., and H.L. Weiner. 2005. Oral tolerance. *Immunological Reviews*. 206:232–259.
646 doi:10.1111/j.0105-2896.2005.00280.x.

647 Feng, J., T. Liu, B. Qin, Y. Zhang, and X.S. Liu. 2012. Identifying ChIP-seq enrichment using MACS.
648 *Nature Protocols*. 7:1728–1740. doi:10.1038/nprot.2012.101.

649 Fernandez, I., R. Zeiser, H. Karsunky, N. Kambham, A. Beilhack, K. Soderstrom, R.S. Negrin, and E.
650 Engleman. 2007. CD101 Surface Expression Discriminates Potency Among Murine FoxP3+
651 Regulatory T Cells. *The Journal of Immunology*. 179:2808–2814.
652 doi:10.4049/jimmunol.179.5.2808.

653 Ferraro, A., A.M. D'Alise, T. Raj, N. Asinovski, R. Phillips, A. Ergun, J.M. Replogle, A. Bernier, L.
654 Laffel, B.E. Stranger, P.L. De Jager, D. Mathis, and C. Benoist. 2014. Interindividual variation in
655 human T regulatory cells. *Proc. Natl. Acad. Sci. U.S.A.* 111. doi:10.1073/pnas.1401343111.

656 Francisco, L.M., V.H. Salinas, K.E. Brown, V.K. Vanguri, G.J. Freeman, V.K. Kuchroo, and A.H.
657 Sharpe. 2009. PD-L1 regulates the development, maintenance, and function of induced regulatory
658 T cells. *Journal of Experimental Medicine*. 206:3015–3029. doi:10.1084/jem.20090847.

659 Hadis, U., B. Wahl, O. Schulz, M. Hardtke-Wolenski, A. Schippers, N. Wagner, W. Müller, T.
660 Sparwasser, R. Förster, and O. Pabst. 2011. Intestinal Tolerance Requires Gut Homing and
661 Expansion of FoxP3+ Regulatory T Cells in the Lamina Propria. *Immunity*. 34:237–246.
662 doi:10.1016/j.immuni.2011.01.016.

663 Hao, Y., S. Hao, E. Andersen-Nissen, W.M. Mauck, S. Zheng, A. Butler, M.J. Lee, A.J. Wilk, C. Darby,
664 M. Zager, P. Hoffman, M. Stoeckius, E. Papalexi, E.P. Mimitou, J. Jain, A. Srivastava, T. Stuart,
665 L.M. Fleming, B. Yeung, A.J. Rogers, J.M. McElrath, C.A. Blish, R. Gottardo, P. Smibert, and R.
666 Satija. 2021. Integrated analysis of multimodal single-cell data. *Cell*. 184:3573-3587.e29.
667 doi:10.1016/j.cell.2021.04.048.

668 Heinz, S., C. Benner, N. Spann, E. Bertolino, Y.C. Lin, P. Laslo, J.X. Cheng, C. Murre, H. Singh, and
669 C.K. Glass. 2010. Simple Combinations of Lineage-Determining Transcription Factors Prime cis-
670 Regulatory Elements Required for Macrophage and B Cell Identities. *Molecular Cell*. 38:576–589.
671 doi:10.1016/j.molcel.2010.05.004.

672 Hong, S.-W., P.D. Krueger, K.C. Osum, T. Dileepan, A. Herman, D.L. Mueller, and M.K. Jenkins. 2022.
673 Immune tolerance of food is mediated by layers of CD4+ T cell dysfunction. *Nature*. 607:762–768.
674 doi:10.1038/s41586-022-04916-6.

675 Hsieh, C.-S., H.-M. Lee, and C.-W.J. Lio. 2012. Selection of regulatory T cells in the thymus. *Nat Rev*
676 *Immunol*. 12:157–167. doi:10.1038/nri3155.

677 Hsieh, C.-S., Y. Liang, A.J. Tyznik, S.G. Self, D. Liggitt, and A.Y. Rudensky. 2004. Recognition of the
678 Peripheral Self by Naturally Arising CD25+ CD4+ T Cell Receptors. *Immunity*. 21:267–277.
679 doi:10.1016/j.immuni.2004.07.009.

680 Hudson, W.H., J. Gensheimer, M. Hashimoto, A. Wieland, R.M. Valanparambil, P. Li, J.-X. Lin, B.T.
681 Konieczny, S.J. Im, G.J. Freeman, W.J. Leonard, H.T. Kissick, and R. Ahmed. 2019. Proliferating
682 Transitory T Cells with an Effector-like Transcriptional Signature Emerge from PD-1+ Stem-like
683 CD8+ T Cells during Chronic Infection. *Immunity*. 51:1043-1058.e4.
684 doi:10.1016/j.immuni.2019.11.002.

685 Josefowicz, S.Z., L.-F. Lu, and A.Y. Rudensky. 2012. Regulatory T Cells: Mechanisms of
686 Differentiation and Function. *Annu. Rev. Immunol.* 30:531–564.
687 doi:10.1146/annurev.immunol.25.022106.141623.

688 Kaminski, A., F.T. Hager, L. Kopplin, F. Ticconi, A. Leufgen, E. Vendelova, L. Rüttger, G. Gasteiger,
689 V. Cerovic, W. Kastenmüller, O. Pabst, and M. Ugur. 2023. Resident regulatory T cells reflect the
690 immune history of individual lymph nodes. *Sci. Immunol.* 8:eadj5789.
691 doi:10.1126/sciimmunol.adj5789.

692 Kawakami, R., Y. Kitagawa, K.Y. Chen, M. Arai, D. Ohara, Y. Nakamura, K. Yasuda, M. Osaki, N.
693 Mikami, C.A. Lareau, H. Watanabe, G. Kondoh, K. Hirota, N. Ohkura, and S. Sakaguchi. 2021.
694 Distinct Foxp3 enhancer elements coordinate development, maintenance, and function of
695 regulatory T cells. *Immunity*. 54:947-961.e8. doi:10.1016/j.immuni.2021.04.005.

696 Kim, J.M., J.P. Rasmussen, and A.Y. Rudensky. 2007. Regulatory T cells prevent catastrophic
697 autoimmunity throughout the lifespan of mice. *Nature Immunology*. 8:191–197.
698 doi:10.1038/ni1428.

699 Kitagawa, Y., N. Ohkura, Y. Kidani, A. Vandenbon, K. Hirota, R. Kawakami, K. Yasuda, D. Motooka,
700 S. Nakamura, M. Kondo, I. Taniuchi, T. Kohwi-Shigematsu, and S. Sakaguchi. 2017. Guidance of
701 regulatory T cell development by Satb1-dependent super-enhancer establishment. *Nature*
702 *Immunology*. 18:173–183. doi:10.1038/ni.3646.

703 Lack, G. 2008. Epidemiologic risks for food allergy. *Journal of Allergy and Clinical Immunology*.
704 121:1331–1336. doi:10.1016/j.jaci.2008.04.032.

705 Langmead, B., and S.L. Salzberg. 2012. Fast gapped-read alignment with Bowtie 2. *Nature Methods*.
706 9:357–359. doi:10.1038/nmeth.1923.

707 Li, B., and C.N. Dewey. 2011. RSEM: accurate transcript quantification from RNA-Seq data with or
708 without a reference genome. *BMC Bioinformatics*. 12:323. doi:10.1186/1471-2105-12-323.

709 Li, H., B. Handsaker, A. Wysoker, T. Fennell, J. Ruan, N. Homer, G. Marth, G. Abecasis, and R. Durbin.
710 2009. The Sequence Alignment/Map format and SAMtools. *Bioinformatics*. 25:2078–2079.
711 doi:10.1093/bioinformatics/btp352.

712 Liao, Y., G.K. Smyth, and W. Shi. 2014. FeatureCounts: An efficient general purpose program for
713 assigning sequence reads to genomic features. *Bioinformatics*. 30:923–930.
714 doi:10.1093/bioinformatics/btt656.

715 Love, M.I., W. Huber, and S. Anders. 2014. Moderated estimation of fold change and dispersion for
716 RNA-seq data with DESeq2. *Genome Biology*. 15:1–21. doi:10.1186/s13059-014-0550-8.

717 Lutz, M.B., R.A. Backer, and B.E. Clausen. 2021. Revisiting Current Concepts on the Tolerogenicity of
718 Steady-State Dendritic Cell Subsets and Their Maturation Stages. *The Journal of Immunology*.
719 206:1681–1689. doi:10.4049/jimmunol.2001315.

720 Mattner, J., J.P. Mohammed, M.E. Fusakio, C. Giessler, C.-P. Hackstein, R. Opoka, M. Wrage, R. Schey,
721 J. Clark, H.I. Fraser, D.B. Rainbow, and L.S. Wicker. 2019. Genetic and functional data identifying
722 Cd101 as a type 1 diabetes (T1D) susceptibility gene in nonobese diabetic (NOD) mice. *PLoS*
723 *Genet*. 15:e1008178. doi:10.1371/journal.pgen.1008178.

724 Mazzini, E., L. Massimiliano, G. Penna, and M. Rescigno. 2014. Oral Tolerance Can Be Established via
725 Gap Junction Transfer of Fed Antigens from CX3CR1+ Macrophages to CD103+ Dendritic Cells.
726 *Immunity*. 40:248–261. doi:10.1016/j.immuni.2013.12.012.

727 Mikami, N., R. Kawakami, K.Y. Chen, A. Sugimoto, N. Ohkura, and S. Sakaguchi. 2020. Epigenetic
728 conversion of conventional T cells into regulatory T cells by CD28 signal deprivation. *Proceedings*
729 *of the National Academy of Sciences of the United States of America*. 117.
730 doi:10.1073/pnas.1922600117.

731 Miragaia, R.J., T. Gomes, A. Chomka, L. Jardine, A. Riedel, A.N. Hegazy, N. Whibley, A. Tucci, X.
732 Chen, I. Lindeman, G. Emerton, T. Krausgruber, J. Shields, M. Haniffa, F. Powrie, and S.A.
733 Teichmann. 2019. Single-Cell Transcriptomics of Regulatory T Cells Reveals Trajectories of
734 Tissue Adaptation. *Immunity*. 50:493-504.e7. doi:10.1016/j.immuni.2019.01.001.

735 Miyara, M., Y. Yoshioka, A. Kitoh, T. Shima, K. Wing, A. Niwa, C. Parizot, C. Taflin, T. Heike, D.
736 Valeyre, A. Mathian, T. Nakahata, T. Yamaguchi, T. Nomura, M. Ono, Z. Amoura, G. Gorochov,
737 and S. Sakaguchi. 2009. Functional Delineation and Differentiation Dynamics of Human CD4+ T
738 Cells Expressing the FoxP3 Transcription Factor. *Immunity*. 30:899–911.
739 doi:10.1016/j.immuni.2009.03.019.

740 Morelli, A.E., and A.W. Thomson. 2007. Tolerogenic dendritic cells and the quest for transplant
741 tolerance. *Nat Rev Immunol*. 7:610–621. doi:10.1038/nri2132.

742 Mowat, A.McI. 2018. To respond or not to respond — a personal perspective of intestinal tolerance. *Nat*
743 *Rev Immunol*. 18:405–415. doi:10.1038/s41577-018-0002-x.

744 Mucida, D., N. Kutchukhidze, A. Erazo, M. Russo, J.J. Lafaille, and M.A. Curotto De Lafaille. 2005.
745 Oral tolerance in the absence of naturally occurring Tregs. *Journal of Clinical Investigation*.
746 115:1923–1933. doi:10.1172/JCI24487.

747 Mucida, D., Y. Park, G. Kim, O. Turovskaya, I. Scott, M. Kronenberg, and H. Cheroutre. 2007.
748 Reciprocal T_H 17 and Regulatory T Cell Differentiation Mediated by Retinoic Acid. *Science*.
749 317:256–260. doi:10.1126/science.1145697.

750 Muñoz-Rojas, A.R., and D. Mathis. 2021. Tissue regulatory T cells: regulatory chameleons. *Nat Rev*
751 *Immunol*. 21:597–611. doi:10.1038/s41577-021-00519-w.

752 Ohkura, N., M. Hamaguchi, H. Morikawa, K. Sugimura, A. Tanaka, Y. Ito, M. Osaki, Y. Tanaka, R.
753 Yamashita, N. Nakano, J. Huehn, H.J. Fehling, T. Sparwasser, K. Nakai, and S. Sakaguchi. 2012. T
754 Cell Receptor Stimulation-Induced Epigenetic Changes and Foxp3 Expression Are Independent
755 and Complementary Events Required for Treg Cell Development. *Immunity*. 37:785–799.
756 doi:10.1016/j.immuni.2012.09.010.

757 Onishi, Y., Z. Fehervari, T. Yamaguchi, and S. Sakaguchi. 2008. $Foxp3^+$ natural regulatory T cells
758 preferentially form aggregates on dendritic cells *in vitro* and actively inhibit their maturation. *Proc.*
759 *Natl. Acad. Sci. U.S.A.* 105:10113–10118. doi:10.1073/pnas.0711106105.

760 Oxley, E.P., N.J. Kershaw, C. Louis, K.J. Goodall, M.M. Garwood, S.M. Jee Ho, V.T.F. Voo, H.-Y.
761 Park, J. Iaria, L.L.L. Wong, A.G. Lebenbaum, S. Wiranata, E.S. Pang, E.S.J. Edwards, D.B.
762 D'Silva, J. Hansen, M.C. Van Zelm, M. O'Keeffe, P.M. Hogarth, N.M. Haynes, N.D. Huntington,

763 I.P. Wicks, and R.A. Dickins. 2024. Context-restricted PD-(L)1 checkpoint agonism by CTLA4-Ig
764 therapies inhibits T cell activity. *Cell Reports*. 43:114834. doi:10.1016/j.celrep.2024.114834.
765 Quinlan, A.R., and I.M. Hall. 2010. BEDTools: A flexible suite of utilities for comparing genomic
766 features. *Bioinformatics*. 26:841–842. doi:10.1093/bioinformatics/btq033.
767 Qureshi, O.S., Y. Zheng, K. Nakamura, K. Attridge, C. Manzotti, E.M. Schmidt, J. Baker, L.E. Jeffery,
768 S. Kaur, Z. Briggs, T.Z. Hou, C.E. Futter, G. Anderson, L.S.K. Walker, and D.M. Sansom. 2011.
769 Trans-Endocytosis of CD80 and CD86: A Molecular Basis for the Cell-Extrinsic Function of
770 CTLA-4. *Science*. 332:600–603. doi:10.1126/science.1202947.
771 Rainbow, D.B., C. Moule, H.I. Fraser, J. Clark, S.K. Howlett, O. Burren, M. Christensen, V. Moody,
772 C.A. Steward, J.P. Mohammed, M.E. Fusakio, E.L. Masteller, E.B. Finger, J.P. Houchins, D. Naf,
773 F. Koentgen, W.M. Ridgway, J.A. Todd, J.A. Bluestone, L.B. Peterson, J. Mattner, and L.S.
774 Wicker. 2011. Evidence that *Cd101* Is an Autoimmune Diabetes Gene in Nonobese Diabetic Mice.
775 *The Journal of Immunology*. 187:325–336. doi:10.4049/jimmunol.1003523.
776 Ramírez, F., D.P. Ryan, B. Grüning, V. Bhardwaj, F. Kilpert, A.S. Richter, S. Heyne, F. Dündar, and T.
777 Manke. 2016. deepTools2: a next generation web server for deep-sequencing data analysis. *Nucleic*
778 *Acids Research*. 44:W160–W165. doi:10.1093/NAR/GKW257.
779 Reeves, P.G., F.H. Nielsen, and G.C. Fahey. 1993. AIN-93 Purified Diets for Laboratory Rodents: Final
780 Report of the American Institute of Nutrition Ad Hoc Writing Committee on the Reformulation of
781 the AIN-76A Rodent Diet. *The Journal of Nutrition*. 123:1939–1951. doi:10.1093/jn/123.11.1939.
782 Rezende, R.M., and H.L. Weiner. 2022. Oral tolerance: an updated review. *Immunology Letters*.
783 245:29–37. doi:10.1016/j.imlet.2022.03.007.
784 Robinson, M.A., A. Kennedy, C.T. Orozco, H.-C. Chen, E. Waters, D. Giovacchini, K. Yeung, L. Filer,
785 C. Hinze, C. Lloyd, S.J. Dovedi, and D.M. Sansom. 2024. Rigid, bivalent CTLA-4 binding to
786 CD80 is required to disrupt the cis CD80/PD-L1 interaction. *Cell Reports*. 43:114768.
787 doi:10.1016/j.celrep.2024.114768.
788 Sakaguchi, S., N. Mikami, J.B. Wing, A. Tanaka, K. Ichiyama, and N. Ohkura. 2020. Regulatory T
789 Cells and Human Disease. *Annual Review of Immunology*. 38:541–566.
790 doi:doi.org/10.1146/annurev-immunol-042718-041717.
791 Schey, R., H. Dornhoff, J.L.C. Baier, M. Purtak, R. Opoka, A.K. Koller, R. Atreya, T.T. Rau, C. Daniel,
792 K. Amann, C. Bogdan, and J. Mattner. 2016. CD101 inhibits the expansion of colitogenic T cells.
793 *Mucosal Immunology*. 9:1205–1217. doi:10.1038/mi.2015.139.
794 Schiering, C., T. Krausgruber, A. Chomka, A. Fröhlich, K. Adelmann, E.A. Wohlfert, J. Pott, T. Griseri,
795 J. Bollrath, A.N. Hegazy, O.J. Harrison, B.M.J. Owens, M. Löhning, Y. Belkaid, P.G. Fallon, and F.
796 Powrie. 2014. The alarmin IL-33 promotes regulatory T-cell function in the intestine. *Nature*.
797 513:564–568. doi:10.1038/nature13577.
798 Shahinian, A., K. Pfeffer, K.P. Lee, T.M. Kündig, K. Kishihara, A. Wakeham, K. Kawai, P.S. Ohashi,
799 C.B. Thompson, and T.W. Mak. 1993. Differential T Cell Costimulatory Requirements in CD28-
800 Deficient Mice. *Science*. 261:609–612. doi:10.1126/science.7688139.
801 Shimura, S., T. Takai, H. Iida, N. Maruyama, H. Ochi, S. Kamijo, I. Nishioka, M. Hara, A. Matsuda, H.
802 Saito, S. Nakae, H. Ogawa, K. Okumura, and S. Ikeda. 2016. Epicutaneous Allergic Sensitization
803 by Cooperation between Allergen Protease Activity and Mechanical Skin Barrier Damage in Mice.
804 *Journal of Investigative Dermatology*. 136:1408–1417. doi:10.1016/j.jid.2016.02.810.
805 Soares, L.R.B., L. Tsavaler, A. Rivas, and E.G. Engleman. 1998. V7 (CD101) Ligation Inhibits
806 TCR/CD3-Induced IL-2 Production by Blocking Ca2+ Flux and Nuclear Factor of Activated T Cell

807 Nuclear Translocation. *The Journal of Immunology*. 161:209–217.
808 doi:10.4049/jimmunol.161.1.209.

809 Sun, C.-M., J.A. Hall, R.B. Blank, N. Bouladoux, M. Oukka, J.R. Mora, and Y. Belkaid. 2007. Small
810 intestine lamina propria dendritic cells promote de novo generation of Foxp3 T reg cells via
811 retinoic acid. *The Journal of Experimental Medicine*. 204:1775–1785. doi:10.1084/jem.20070602.

812 Szurek, E., A. Cebula, L. Wojciech, M. Pietrzak, G. Rempala, P. Kisielow, and L. Ignatowicz. 2015.
813 Differences in Expression Level of Helios and Neuropilin-1 Do Not Distinguish Thymus-Derived
814 from Extrathymically-Induced CD4+Foxp3+ Regulatory T Cells. *PLoS ONE*. 10:e0141161.
815 doi:10.1371/journal.pone.0141161.

816 Tanoue, T., K. Atarashi, and K. Honda. 2016. Development and maintenance of intestinal regulatory T
817 cells. *Nat Rev Immunol*. 16:295–309. doi:10.1038/nri.2016.36.

818 Tekguc, M., J.B. Wing, M. Osaki, J. Long, and S. Sakaguchi. 2021. Treg-expressed CTLA-4 depletes
819 CD80/CD86 by trogocytosis, releasing free PD-L1 on antigen-presenting cells. *Proc. Natl. Acad.*
820 *Sci. U.S.A.* 118:e2023739118. doi:10.1073/pnas.2023739118.

821 Thornton, A.M., P.E. Korty, D.Q. Tran, E.A. Wohlfert, P.E. Murray, Y. Belkaid, and E.M. Shevach.
822 2010. Expression of Helios, an Ikaros Transcription Factor Family Member, Differentiates Thymic-
823 Derived from Peripherally Induced Foxp3+ T Regulatory Cells. *The Journal of Immunology*.
824 184:3433–3441. doi:10.4049/jimmunol.0904028.

825 Thornton, A.M., and E.M. Shevach. 2019. Helios: still behind the clouds. *Immunology*. 158:161–170.
826 doi:10.1111/imm.13115.

827 Tsui, C., L. Kretschmer, S. Rapelius, S.S. Gabriel, D. Chisanga, K. Knöpper, D.T. Utzschneider, S.
828 Nüssing, Y. Liao, T. Mason, S.V. Torres, S.A. Wilcox, K. Kanev, S. Jarosch, J. Leube, S.L. Nutt, D.
829 Zehn, I.A. Parish, W. Kastenmüller, W. Shi, V.R. Buchholz, and A. Kallies. 2022. MYB
830 orchestrates T cell exhaustion and response to checkpoint inhibition. *Nature*. 609:354–360.
831 doi:10.1038/s41586-022-05105-1.

832 Van Wijk, F., S. Hoeks, S. Nierkens, S.J. Koppelman, P. Van Kooten, L. Boon, L.M.J. Knippels, and R.
833 Pieters. 2005. CTLA-4 Signaling Regulates the Intensity of Hypersensitivity Responses to Food
834 Antigens, but is Not Decisive in the Induction of Sensitization. *The Journal of Immunology*.
835 174:174–179. doi:10.4049/jimmunol.174.1.174.

836 Wang, L., K. Pino-Lagos, V.C. De Vries, I. Guleria, M.H. Sayegh, and R.J. Noelle. 2008. Programmed
837 death 1 ligand signaling regulates the generation of adaptive Foxp3+ CD4+ regulatory T cells. *Proc.*
838 *Natl. Acad. Sci. U.S.A.* 105:9331–9336. doi:10.1073/pnas.0710441105.

839 Weiss, J.M., A.M. Bilate, M. Gobert, Y. Ding, M.A. Curotto De Lafaille, C.N. Parkhurst, H. Xiong, J.
840 Dolpady, A.B. Frey, M.G. Ruocco, Y. Yang, S. Floess, J. Huehn, S. Oh, M.O. Li, R.E. Niec, A.Y.
841 Rudensky, M.L. Dustin, D.R. Littman, and J.J. Lafaille. 2012. Neuropilin 1 is expressed on
842 thymus-derived natural regulatory T cells, but not mucosa-generated induced Foxp3+ T reg cells.
843 *Journal of Experimental Medicine*. 209:1723–1742. doi:10.1084/jem.20120914.

844 Windom, R.R., S. Seitz, J.B. Ly, N. Dunn, J. Fergeson, and H.H. Windom. 2024. Food Sublingual
845 Immunotherapy: Safety and Simplicity of a Real Food Updosing Protocol. *The Journal of Allergy*
846 *and Clinical Immunology: In Practice*. 12:2447-2453.e1. doi:10.1016/j.jaip.2024.05.007.

847 Wing, K., Y. Onishi, P. Prieto-Martin, T. Yamaguchi, M. Miyara, Z. Fehervari, T. Nomura, and S.
848 Sakaguchi. 2008. CTLA-4 Control over Foxp3^{+} Regulatory T Cell Function. *Science*. 322:271–275.
849 doi:10.1126/science.1160062.

850 Wu, T., E. Hu, S. Xu, M. Chen, P. Guo, Z. Dai, T. Feng, L. Zhou, W. Tang, L. Zhan, X. Fu, S. Liu, X.
851 Bo, and G. Yu. 2021. clusterProfiler 4.0: A universal enrichment tool for interpreting omics data.
852 *The Innovation*. 2:100141. doi:10.1016/j.xinn.2021.100141.

853 Yuan, J., R.B. Crittenden, and T.P. Bender. 2010. c-Myb Promotes the Survival of CD4+CD8+ Double-
854 Positive Thymocytes through Upregulation of Bcl-xL. *The Journal of Immunology*. 184:2793–2804.
855 doi:10.4049/jimmunol.0902846.

856 Zheng, S.G., J.D. Gray, K. Ohtsuka, S. Yamagiwa, and D.A. Horwitz. 2002. Generation Ex Vivo of
857 TGF-β-Producing Regulatory T Cells from CD4+CD25–Precursors. *The Journal of Immunology*.
858 169:4183–4189. doi:10.4049/jimmunol.169.8.4183.

859

860 **Figure legends**

861 **Fig. 1. pTreg generation and maintenance by antigen feeding in establishing oral tolerance.** (**A**)
862 Antigen feeding to DORe mice and assessment of ear swelling upon antigen challenge. (**B**) Changes in
863 right ear thickness in DORe mice treated as shown in (A). Arrowheads indicate OVA challenges. (**C**)
864 Histology of right ear and histological scores in NC- or EWP-fed DORe mice. Bars in histology indicate
865 100 μm. (**D**) CD25 and Foxp3 expression by DO $CD4^+$ T cells in mLNs, dLNs, and both ears. Barplots
866 indicate frequencies of $Foxp3^+$ cells (pTreg cells) (n = 10 and 11). (**E-G**) Treg cell depletion in EWP-fed
867 DORF mice. Mice were treated twice with DTx followed by OVA challenge (E). Ear thickness and
868 histological scores (F). Frequencies of pTreg cells in the right ear (G) (n = 5-7). (**H-J**) Cessation of EWP
869 feeding for 4 weeks (designated EWP(-)4wk) or 8 weeks (EWP(-)8wk) before OVA challenge (H). Ear
870 thickness and histological scores (I). Frequencies of pTreg cells in right ear (J) (n = 4-6). (**K**-**N**) Effects
871 of skin OVA sensitization and subsequent OVA feeding on ear swelling upon OVA challenge (K). Ear
872 thickness and histological scores (L). Frequencies of pTreg cells in right ear (M) (n = 5 and 6). Changes
873 in body weight of DORe mice (N). Vertical bars indicate mean ± SEM. Statistical significance was
874 assessed by unpaired t test or Welch's t test (B, C, D, F, G, L, M, N), and Tukey-Kramer test (I, J).

875 **Fig. 2. Antigen-dependent development of pTreg cells with Treg type epigenome in oral tolerance.**
876 (**A**) Representative CD25 and Foxp3 expression by DO $CD4^+$ T cells in mLNs and SI-LP from DORe
877 mice maintained by designated diet for 6 weeks. (**B, C**) Frequencies of $Foxp3^+$ cells among DO $CD4^+$ T
878 cells (B) and CD25 expression level of $Foxp3^+$ cells (C) in mLNs and SI-LP in the mouse groups as
879 shown in (A) (n = 5-8). (**D**) Degrees of demethylation as percentage of demetylated CpG residues at
880 Treg-specific demethylation regions in *Foxp3*-CNS2, *Ikzf2*, *Ikzf4*, and *Ctla4* loci of pTreg cells in the
881 mice as shown in **A**. (**E**) H3K27ac ChIP-seq signals at global Treg-specific or Tconv-specific enhancer
882 regions in WT or DORe-derived naïve Tconv or Treg cells. (**F**, **G**) H3K27ac ChIP-seq and ATAC-seq
883 peak call at the *Foxp3* gene locus (F) and other Treg-specific enhancer loci at *Ctla4*, *Il2ra*, and *Ikzf2* (G)
884 in eFox-derived naïve Tconv and nTreg cells, DORe-derived naïve Tconv and pTreg cells. Vertical bars
885 indicate mean ± SEM. Statistical significance was assessed by Tukey-Kramer test (B, C).

886 **Fig. 3. Generation of tissue-specific effector-type pTreg cells by antigen feeding.** (**A**) scRNA-seq of
887 DO $CD4^+$ T cells in mice fed with NC- or EWP-food for 4 weeks from weaning. (**B**) Hashtag
888 oligonucleotide (HTO) classification of DO $CD4^+$ T cells in SI-LP in NC- or EWP-fed mice (left) with
889 proportion of cells in each cluster (right). (**C, D**) Volcano plot of differentially expressed genes (C) and
890 gene ontology analysis (D) between Cluster 3 and 5 pTreg cells. (**E**) UMAP plots of cells re-clustered
891 from Clusters 3, 4, 5, 11 shown in (A), with projection of specifically expressed genes. (**F**) UMAP plots
892 with NC- or EWP-derived HTO and *Foxp3* expression, as shown in E. (**G**) Pseudotime trajectory of re-
893 clustered cells in (F). (**H, I**) Contour plots and MFI of 4-1BB and OX40 (H), TIGIT and GITR (I)
894 staining of pTreg cells in SI-LP of NC- or EWP-fed mice (n = 3-6). (**J**) Frequencies of T-bet^+, $GATA3^+$,
895 or $ROR\gamma T^+$ pTreg cells in NC- or EWP-fed mice (n = 4-6 each). (**K**) Ki-67 and KLRG1 expression of
896 SI-LP-derived pTreg cells in DORe mice kept fed with NC or EWP, or ceased to be EWP-fed for 4
897 weeks （EWP (-)4wk） as shown in Fig. 1H (n = 4-5). (**L**) PCA of transcriptomes of pTreg cells from
898 mLNs, dLNs, SI-LP, and ear tissue (n = 3 each). (**M,** and **N**) TPM-normalized *Bcl2* (M), *Ccr9* and *Ccr5*

899 (N) expression by pTreg cells from designated tissues. (**O**) CCR9 and CCR5 expression by SI-LP- and
900 ear tissue-derived pTreg cells. Vertical bars indicate mean ± SEM. Statistical significance was assessed
901 by unpaired *t* test or Welch's *t* test (H, I, J), and Tukey-Kramer test (K).

902 **Fig. 4. Specific expression of CD101 by pTreg cells generated by antigen feeding.** (**A**) Irradiated
903 CD45.1 Rag2KO mice reconstructed with CD3e$^+$ cell-depleted bone marrow cells isolated from WT
904 (Thy1.1-eFox) and DORe mice. Mixed BMC mice were analyzed at 4-8 weeks after BM cell transfer.
905 (**B**-**D**) Representative flow cytometry profiles of WT- and DORe-derived CD4$^+$ T cells in mLNs of
906 BMC mice fed with NC- or EWP-chow for 4 weeks (B). Frequency of WT- and DORe-derived Foxp3$^+$
907 cells in designated tissues (C) (n = 10-12) and in the thymus (n = 8) (D). (**E**) Volcano plot of
908 differentially expressed genes between DORe-pTreg cells and WT-nTreg cells assessed by RNA-seq
909 analysis. (**F, G**) TPM-normalized differentially expressed genes (F) and genes encoding known tTreg-
910 markers (G) in BMC mice as shown in (B) (n = 3). (**H**) CD101 expression by DORe-pTreg cells and
911 WT nTreg cells in BMC mice as shown in (B). Barplots indicate MFI of CD101 expression and
912 frequency of CD101$^+$ cells (n = 6). (**I**) CD101 expression by WT-Treg or Tconv cells, DORe-pTreg or
913 Tconv cells in untreated mice. Barplots indicate MFI of CD101 expression and frequency of CD101$^+$
914 cells (n = 3). Vertical bars indicate mean ± SEM. Statistical significance was assessed by unpaired *t* test
915 or Welch's *t* test (C, H).

916 **Fig. 5. CD101 expression by pTreg cells, thymocytes, and peripheral T cells in WT mice.** (**A**)
917 Experimental scheme for assessing pTreg development in WT mice. Naïve CD4$^+$ T cells from DORe
918 mice were transferred into WT (Thy1.1-eFox) mice, which were then fed with EWP for 3 days. (**B**)
919 Foxp3$^+$CD4$^+$ T cells in transferred DORe CD4$^+$ T cells and in the host. Representative flow cytometry
920 profiles of CD4$^+$ T cells in mLNs of WT mice treated as shown in (A) and frequency of WT- and
921 DORe-derived Foxp3$^+$ cells (n = 4). (**C**) Frequencies and cell numbers of WT- and DORe-derived Treg
922 cells in total CD4$^+$ T cells. (**D**) CD101 and Nrp-1 expression by WT- and DORe-derived Foxp3$^+$ cells.
923 Representative flow cytometry profile and MFI of the expression (n = 4). (**E**) Gating strategy of
924 thymocytes in WT mice. Whole thymocytes (left), CD4/CD8-double-negative (DN) thymocytes
925 (middle), and CD4-single-positive (SP) thymocytes (right). (**F**) CD101 expression by thymocyte
926 subpopulations. Representative histograms and frequencies of CD101$^+$ cells in thymocyte fractions
927 shown in (E) (n = 4). (**G**) Gating strategy of mLN-derived cells in WT mice. (**H**) Representative
928 histogram of CD101 expression and frequencies of CD101$^+$ cells in WT mLN-derived T-cell fractions
929 (n = 6). (**I**, **J**) Representative flowcytometry profiles of CD101 and co-stained T cell-related molecules
930 on Foxp3$^+$ Treg or Foxp3$^-$ T cells from the thymus (I) and mLNs (J). Vertical bars indicate mean ± SEM.

931 **Fig. 6. *In vitro* generation of CD101$^+$ iTreg cells by absence or blockade of costimulatory signal**
932 **during their induction.** (**A**) *In vitro* generation of iTreg cells and their CD101 expression. iTreg cells
933 were induced by plate-bound anti-CD3e mAb with or without anti-CD28 mAb in the presence of TGF-β
934 and IL-2 (n = 3). (**B**) iTreg induction and their CD101 expression by anti-CD3e (0.5, 1, 5, and 10 μg/ml)
935 and anti-CD28 mAb (0, 0.5, 1, and 2 μg/ml) stimulation as in (A) (n = 3). (**C**, **D**) iTreg induction from
936 CD28-deficient or -intact CD4$^+$ T cells (C) and their expression of CD101 (D) as in (A) (n = 3). (**E**, **F**)
937 iTreg generation (E) and CD101 expression (F) by iTreg cells induced by co-culturing DO naïve Tconv

938 cells with SI-LP-derived cDC1 or cDC2 in the presence of OVA and CTLA4-Ig (*n* = 4). (**G**) Effects of
939 inflammatory cytokines (10 ng/ml each) and CTLA4-Ig on antigen-specific iTreg induction and their
940 CD101 expression as in (E) and (F) (*n* = 3). 1 and 2 mean cDC1 and cDC2, respectively. (**H**) iTreg
941 induction from antigen-specific Tconv cells in antigen-sensitized DORe mice. Naïve or effector Tconv
942 cells from dLNs of antigen-sensitized DORe mice were co-cultured with SI-LP-derived cDC1 or cDC2
943 cells in the presence of OVA and CTLA4-Ig. (**I, J**) Frequencies of iTreg cells (I) and CD101 expression
944 (J) of iTreg cells induced as shown in (H) (*n* = 6). Vertical bars indicate mean ± SEM. Statistical
945 significance was assessed by Tukey's HSD test (B) and unpaired *t* test or Welch's *t* test (C, D, E, F, G,
946 J).

947 **Fig. 7. Establishment of oral tolerance in antigen-presensitized mice by CD80/CD86 blockade and**
948 **subsequent antigen feeding.** (**A**) Experimental protocol. DORe mice were OVA sensitized at the right
949 ear four times, i.p. injected with CTLA4-Ig or saline on day 11, fed with EWP chow or NC for four days,
950 OVA challenged at the left ear four times from day 22, and assessed for ear swelling. (**B, C**) Changes in
951 body weight (B), left ear thickness and histological scores (C) (*n* = 5-6). Arrowheads indicate OVA
952 challenges. (**D**, **E**) Frequencies of pTreg cells in mLNs, dLNs, and the right ear at day 15 (D) and day 33
953 (E) (*n* = 5-6). (**F**, **G**) Frequencies of IFN-γ^+, IL-4^+, and IL-$17A^+$ cells in dLNs at day 15 (F) and day 33
954 (G) (*n* = 5-6). (**H**) CD101 expression by pTreg cells in dLNs and the right ear at day 15. Numbers in the
955 histogram are representative of the frequency of $CD101^+$ cells. Barplots indicate the frequency of
956 $CD101^+$ pTreg cells (*n* = 4-10/group). (**I**) Frequencies of $CD101^+$ cells within pTreg cells in dLNs and
957 the left ear at day 33 (*n* = 5-6). (**J**, **K**) Effects of Treg depletion after CTLA4-Ig injection and EWP
958 feeding, After CTLA4-Ig injection and EWP feeding, DORF mice were i.p. treated with PBS or DTx at
959 days 15 and 18, and re-challenged with OVA (arrowheads). Changes in left ear thickness at day 33 in
960 DORF mice (J) (*n* = 6-7). CD101 expression by pTreg cells in mLNs, dLNs, and the left ear (K).
961 Barplots indicate the frequencies of $CD101^+$ pTreg cells (*n* = 3). Vertical bars indicate mean ± SEM.
962 Statistical significance was assessed by Tukey-Kramer test (C, D, E, F, G, H, I) and unpaired *t* test or
963 Welch's *t* test (J, K).

964 **Fig. S1. pTreg generation and maintenance by antigen feeding.** (**A**) The number of DO $CD4^+$ T cells
965 in dLNs in Fig. 1A. (**B**) Frequency of IFN-γ^+, IL-4^+, and IL-$17A^+$ cells among DO $CD4^+$ T cells in dLNs
966 (*n* = 10 and 11). (**C**) CD25 and Foxp3 expression by DO $CD4^+$ T cells in the spleen at 4 weeks after
967 designated feeding (*n* = 4). (**D**) Changes in left ear thickness in Fig. 1A. Arrowheads indicate OVA
968 challenges. (**E**) Histology and histological scores of the left ear in NC- and EWP-fed DORe mice. Bars
969 in histology indicate 100 μm. (**F**, **G**) Frequencies of pTreg cells in mLNs, dLNs, and the right ear (F)
970 and frequencies of IFN-γ^+, IL-4^+, and IL-$17A^+$ cells in dLNs (G) in the mice shown in Fig. 1G (*n* = 7
971 (PBS-treated) or *n* = 6 (DTx-treated)). (**H**, **I**) Frequencies of pTreg cells in mLNs and dLNs (H), and
972 frequencies of IFN-γ^+, IL-4^+, and IL-$17A^+$ cells in dLNs (I) in the mice shown in Fig. 1J (*n* = 4-6). (**J**,
973 **K**) Frequencies of pTreg cells in mLNs and dLNs (J), and frequencies of IFN-γ^+, IL-4^+, and IL-$17A^+$
974 cells in dLNs (K) (*n* = 4-6). Vertical bars indicate mean ± SEM. Statistical significance was assessed by
975 unpaired *t* test or Welch's *t* test (A, B, C, E, F, G, J, K), and Tukey-Kramer test (H, I).

976 **Fig. S2. pTreg cell development at different antigen doses and after depletion of pre-existing**
977 **pTreg cells in NC-fed DORe mice.** (**A**, **B**) CD62L and CD44 expression by pTreg cells (A) and
978 frequencies of $CD44^{hi}CD62L^{lo}$ effector pTreg cells (B) in mLNs and SI-LP from DORe mice fed with
979 designated diets for 6 weeks. (**C, D**) $Foxp3^{+}CD4^{+}$ T cells in the thymus and peripheral lymphoid tissues
980 of NC-fed DORe or WT (eFox) mice. Representative staining for Foxp3/CD25 and the frequencies of
981 $CD25^{+}Foxp3^{+}$ T cells in the thymus and $Foxp3^{+}$ T cells in various tissues (n = 3 for thymus, spleen,
982 pLNs, mLNs, and Peyer's patches (PP)) or (n = 6 for SI-IE, SI-LP, and LI-LP). (**E**) Methylation status in
983 TSDRs of DORe-derived pTreg cells compared to eFox-derived nTreg cells. Empty and black circles
984 indicate demethylated and methylated CpG residues, respectively. (**F**) Helios and Nrp-1 expression
985 levels of eFox-Tconv, DORe-Tconv, eFox-nTreg, and DORe-pTreg cells. Barplots indicate MFI of
986 Helios and Nrp-1 expression on eFox-nTreg cells and DORe-pTreg cells (n = 3). (**G**) *De novo* pTreg
987 development after depletion of pTreg cells preexisting in NC-fed mice. DORF mice having been
988 maintained with NC feeding were DTx-treated and then fed with NC or EWP-chow for 4 weeks. (**H, I**)
989 $Foxp3^{+}CD4^{+}$ T cells immediately after DTx treatment (H) and after EWP or NC feeding for 4 weeks (I).
990 Representative flow cytometry plots and the ratios of $Foxp3^{+}$ pTreg cells in mLNs (n = 3-4). Vertical
991 bars indicate mean ± SEM. Statistical significance was assessed by unpaired t test (I).

992 **Fig. S3. Single-cell RNA-seq analysis of T cells in DORe mice and bulk mRNA-seq analysis of**
993 **pTreg cells from different tissues after EWP feeding.** (**A**) Uniform manifold approximation and
994 projection (UMAP) plots for expression levels of T cell-related molecules in DO $CD4^{+}$ T cells in NC- or
995 EWP-fed DORe mice. (**B**) Marker dotplots of differentially expressed genes in re-clustered T cell
996 clusters in Fig. 3E. (**C**) Marker dotplots of anti-apoptosis and pro-apoptosis related genes in re-clustered
997 T cell clusters. (**D**) Projection of 75 Cluster 3-up-regulated genes detected by scRNA-seq as shown in
998 Fig. 3C on the transcriptome. (**E**) Heatmap of anti-apoptosis and pro-apoptosis related genes among
999 pTreg cells from designated tissues. (**F**) TPM-normalized gene expression of chemokine receptors
1000 among DORe-pTreg cells derived from different tissues. Vertical bars indicate mean ± SEM.

1001 **Fig. S4. Dose effects of CTLA-4-Ig, TGF-β, and IL-2 on iTreg generation.** (**A**) Synergistic effect of
1002 TGF-β supplementation and CD28 signal deprivation on *in vitro* iTreg induction and CD101 expression
1003 by naïve $CD4^{+}$ Tconv cells (n = 4). (**B**) Experimental design. DORe-derived naïve Tconv cells and
1004 splenic DCs were co-cultured with or without CTLA4-Ig in the presence of OVA, TGF-β and IL-2. (**C**)
1005 Response to various concentrations of CTLA4-Ig (0, 2, 10, and 50 μg/ml) in *in vitro* iTreg induction (n
1006 = 4). (**D**) Response to various concentrations of IL-2 (0, 1, 10, and 100 U/ml) in *in vitro* iTreg induction
1007 and CD101 expression (n = 4 (0 U/ml) and n = 7 (1-100 U/ml)). (**E**) Degrees of demethylation as
1008 percentage at *Foxp3*-CNS2 regions of iTreg cells induced with or without CTLA4-Ig. (**F**) Gating
1009 strategy for isolating classic dendritic cells from SI-LP of WT mice. Vertical bars indicate mean ± SEM.
1010 Statistical significance was assessed by unpaired t test or Welch's t test (A, C).

1011 **Fig. S5. Effects of CD80/CD86 blockade and subsequent antigen feeding on antigen-presensitized**
1012 **mice.** (**A**, **B**) Changes in ear thickness of the right ear (A) and body weight (B) of the mice treated as
1013 shown in Fig. 7A. Arrowheads indicate OVA challenges. (**C**) Representative histologies of the left ear of
1014 the mouse groups at day 33 as shown in Fig. 7C. Bars in histology indicate 100 μm. (**D-F**) Experimental

1015 protocol to assess the effects of EWP doses on oral tolerance induction by CTLA4-Ig treatment and
1016 EWP feeding (D). DORe mice were OVA sensitized at the right ear four times, i.p. injected with
1017 CTLA4-Ig on day 11, fed with 1, 10, or 30% EWP chow for four days, OVA challenged at the left ear
1018 four times from day 22, and assessed for body weight (E) and ear swelling (F) (n = 4). (**G**)
1019 Demethylation status and frequencies of demethylation at *Foxp3*-CNS2 locus of DORe pTreg cells
1020 isolated from the mice treated with saline or 10 μg CTLA4-Ig followed by EWP feeding and assessed at
1021 day 15 in Fig. 7A. (**H, I**) Frequencies of pTreg cells in mLNs, dLNs, and left ears (H) and of IFN-γ^+, IL-
1022 4^+, and IL-17A$^+$ cells in dLNs at day 33 in DORF mice treated as described in Fig. 7J (I) (n = 6-7).
1023 Vertical bars indicate mean ± SEM. Statistical significance was assessed by unpaired t test or Welch's t
1024 test (H, I).

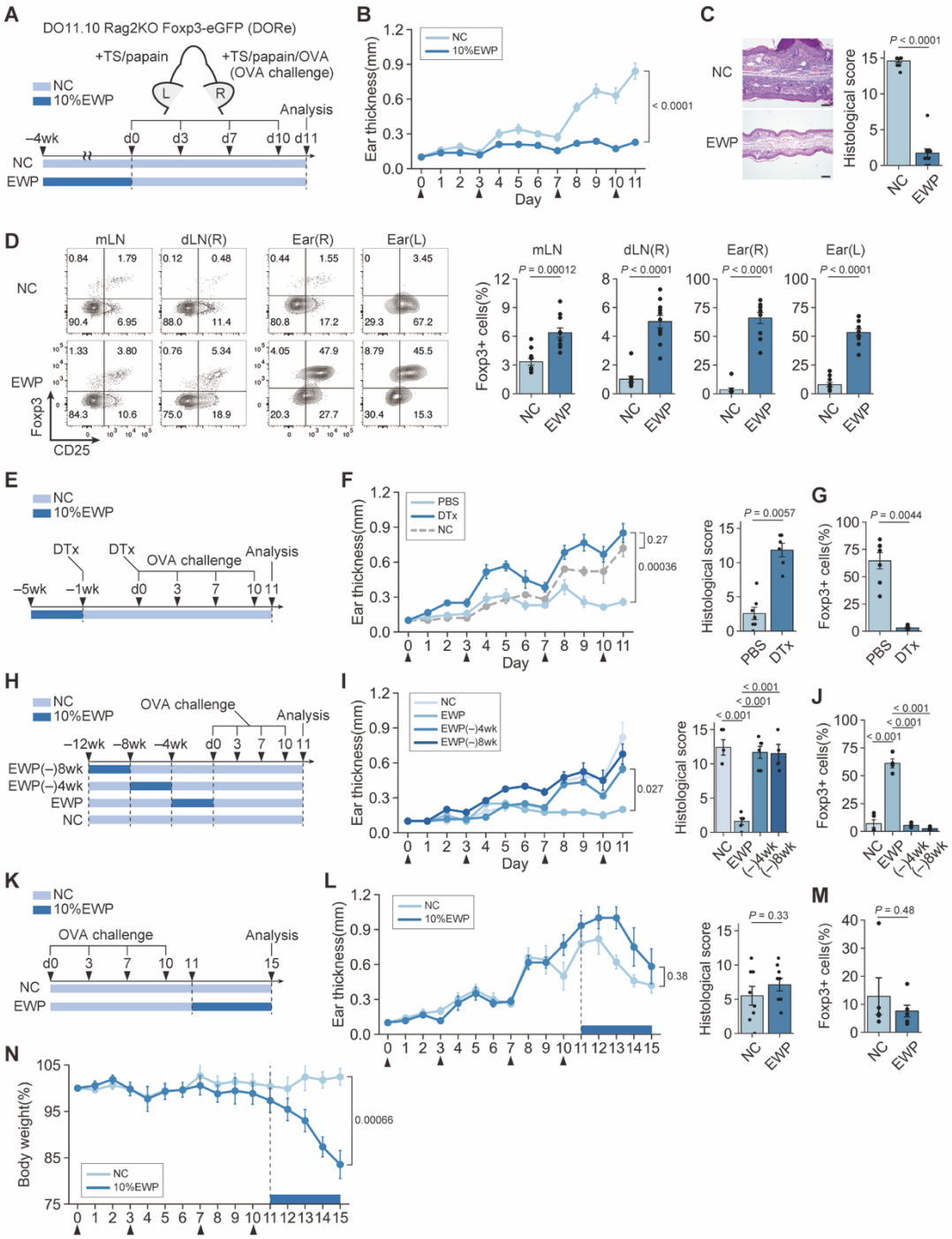
A
DO11.10 Rag2KO Foxp3-eGFP (DORe)
+TS/papain
+TS/papain/OVA (OVA challenge)
NC
10%EWP
L
R
Analysis
–4wk
d0
d3
d7
d10
d11
B
Ear thickness(mm)
Day
< 0.0001
C
P < 0.0001
Histological score
D
mLN
dLN(R)
Ear(R)
Ear(L)
Foxp3
CD25
Foxp3+ cells(%)
P = 0.00012
P < 0.0001
E
DTx
OVA challenge
–5wk
–1wk
F
PBS
0.27
0.00036
G
P = 0.0057
P = 0.0044
H
–12wk
–8wk
EWP(–)8wk
EWP(–)4wk
I
EWP
0.027
J
< 0.001
K
L
0.38
M
P = 0.33
P = 0.48
N
Body weight(%)
0.00066

Fig. 1

1025

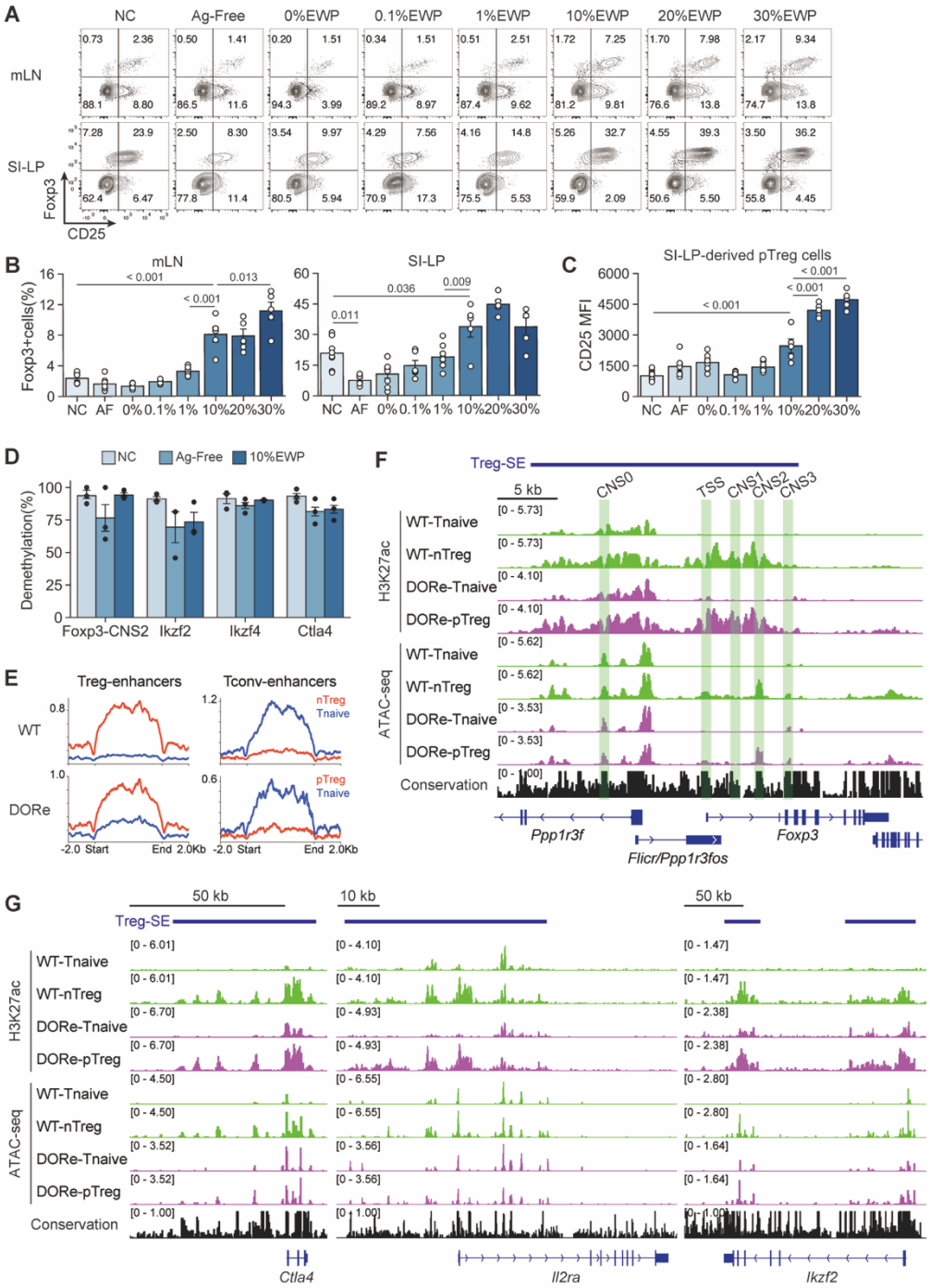
A
NC
Ag-Free
0%EWP
0.1%EWP
1%EWP
10%EWP
20%EWP
30%EWP
mLN
SI-LP
Foxp3
CD25
B
mLN
SI-LP
Foxp3+cells(%)
NC AF 0% 0.1% 1% 10% 20% 30%
C
SI-LP-derived pTreg cells
CD25 MFI
D
NC
Ag-Free
10%EWP
Demethylation(%)
Foxp3-CNS2
Ikzf2
Ikzf4
Ctla4
E
Treg-enhancers
Tconv-enhancers
WT
DORe
nTreg
Tnaive
pTreg
Tnaive
-2.0 Start
End 2.0Kb
F
Treg-SE
5 kb
CNS0
TSS
CNS1
CNS2
CNS3
H3K27ac
ATAC-seq
WT-Tnaive
WT-nTreg
DORe-Tnaive
DORe-pTreg
Conservation
Ppp1r3f
Flicr/Ppp1r3fos
Foxp3
G
50 kb
10 kb
50 kb
Treg-SE
Ctla4
Il2ra
Ikzf2

Fig. 2

1026

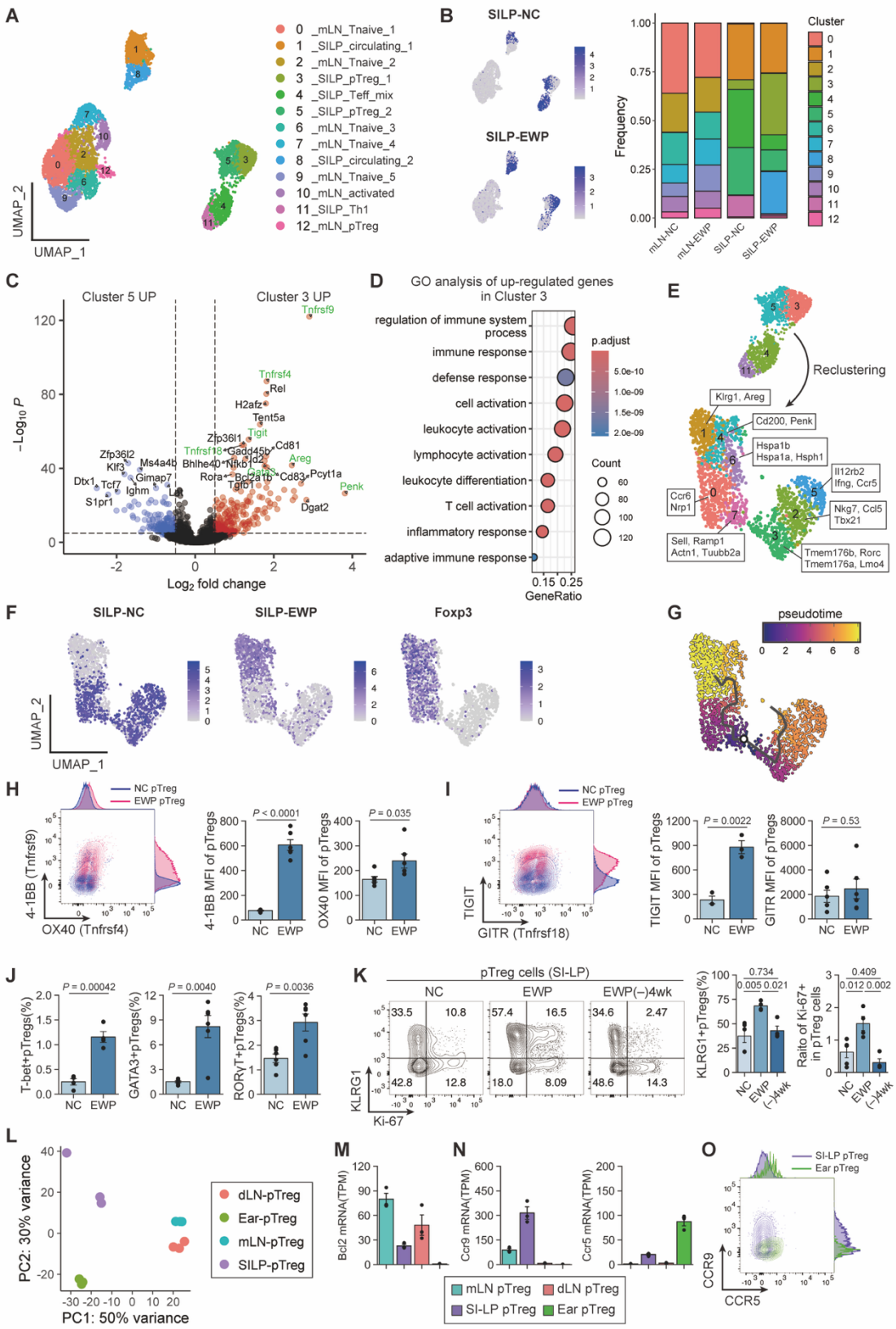
A
0 _mLN_Tnaive_1
1 _SILP_circulating_1
2 _mLN_Tnaive_2
3 _SILP_pTreg_1
4 _SILP_Teff_mix
5 _SILP_pTreg_2
6 _mLN_Tnaive_3
7 _mLN_Tnaive_4
8 _SILP_circulating_2
9 _mLN_Tnaive_5
10 _mLN_activated
11 _SILP_Th1
12 _mLN_pTreg
UMAP_2
UMAP_1
B
SILP-NC
SILP-EWP
Frequency
Cluster
mLN-NC
mLN-EWP
SILP-NC
SILP-EWP
C
Cluster 5 UP
Cluster 3 UP
Tnfrsf9
Tnfrsf4
Rel
H2afz
Tent5a
Tigit
Cd81
Areg
Penk
Dgat2
Zfp36l2
Klf3
Ms4a4b
Gimap7
Dtx1
Tcf7
Ighm
S1pr1
Log2 fold change
-Log10 P
D
GO analysis of up-regulated genes in Cluster 3
regulation of immune system process
immune response
defense response
cell activation
leukocyte activation
lymphocyte activation
leukocyte differentiation
T cell activation
inflammatory response
adaptive immune response
p.adjust
Count
GeneRatio
E
Reclustering
Klrg1, Areg
Cd200, Penk
Hspa1b
Hspa1a, Hsph1
Il12rb2
Ifng, Ccr5
Ccr6
Nrp1
Nkg7, Ccl5
Tbx21
Sell, Ramp1
Actn1, Tuubb2a
Tmem176b, Rorc
Tmem176a, Lmo4
F
SILP-NC
SILP-EWP
Foxp3
UMAP_2
UMAP_1
G
pseudotime
H
NC pTreg
EWP pTreg
4-1BB (Tnfrsf9)
OX40 (Tnfrsf4)
4-1BB MFI of pTregs
OX40 MFI of pTregs
P < 0.0001
P = 0.035
NC
EWP
I
NC pTreg
EWP pTreg
TIGIT
GITR (Tnfrsf18)
TIGIT MFI of pTregs
GITR MFI of pTregs
P = 0.0022
P = 0.53
J
T-bet+pTregs(%)
GATA3+pTregs(%)
RORγT+pTregs(%)
P = 0.00042
P = 0.0040
P = 0.0036
K
pTreg cells (SI-LP)
NC
EWP
EWP(−)4wk
33.5
10.8
42.8
12.8
57.4
16.5
18.0
8.09
34.6
2.47
48.6
14.3
KLRG1
Ki-67
KLRG1+pTregs(%)
Raito of Ki-67+ in pTreg cells
0.734
0.005 0.021
0.409
0.012 0.002
L
PC2: 30% variance
PC1: 50% variance
dLN-pTreg
Ear-pTreg
mLN-pTreg
SILP-pTreg
M
Bcl2 mRNA(TPM)
N
Ccr9 mRNA(TPM)
Ccr5 mRNA(TPM)
mLN pTreg
dLN pTreg
SI-LP pTreg
Ear pTreg
O
SI-LP pTreg
Ear pTreg
CCR9
CCR5

Fig. 3

1027

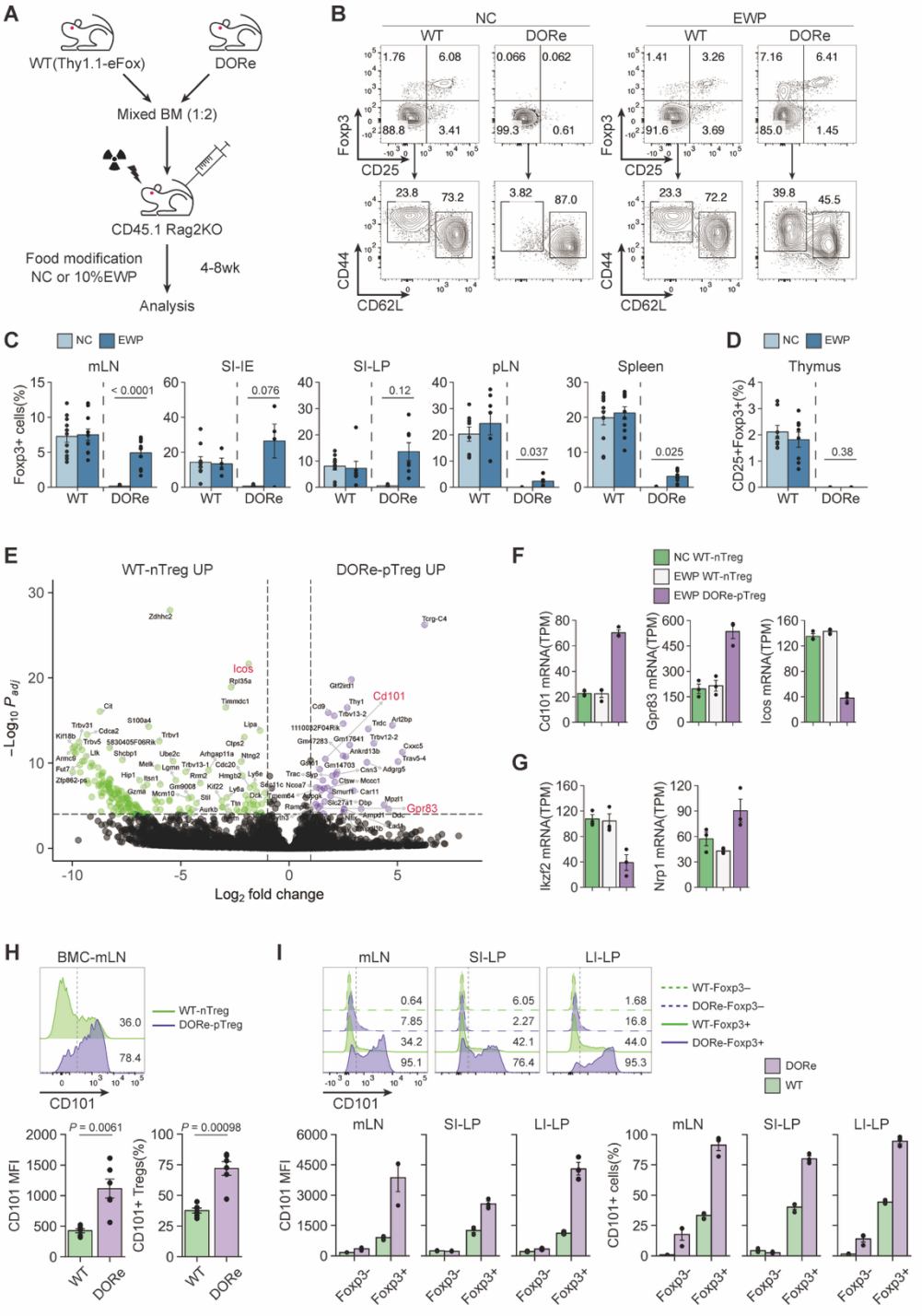
A
WT(Thy1.1-eFox)
DORe
Mixed BM (1:2)
CD45.1 Rag2KO
Food modification
NC or 10%EWP
4-8wk
Analysis
B
NC
EWP
WT
DORe
Foxp3
CD25
CD44
CD62L
C
NC
EWP
mLN
SI-IE
SI-LP
pLN
Spleen
Foxp3+ cells(%)
< 0.0001
0.076
0.12
0.037
0.025
D
Thymus
CD25+Foxp3+(%)
0.38
E
WT-nTreg UP
DORe-pTreg UP
Icos
Cd101
Gpr83
Log2 fold change
F
NC WT-nTreg
EWP WT-nTreg
EWP DORe-pTreg
Cd101 mRNA(TPM)
Gpr83 mRNA(TPM)
Icos mRNA(TPM)
G
Ikzf2 mRNA(TPM)
Nrp1 mRNA(TPM)
H
BMC-mLN
WT-nTreg
DORe-pTreg
CD101
CD101 MFI
P = 0.0061
CD101+ Tregs(%)
P = 0.00098
I
mLN
SI-LP
LI-LP
WT-Foxp3–
DORe-Foxp3–
WT-Foxp3+
DORe-Foxp3+
DORe
WT
CD101 MFI
CD101+ cells(%)
Foxp3-
Foxp3+

Fig. 4

1028

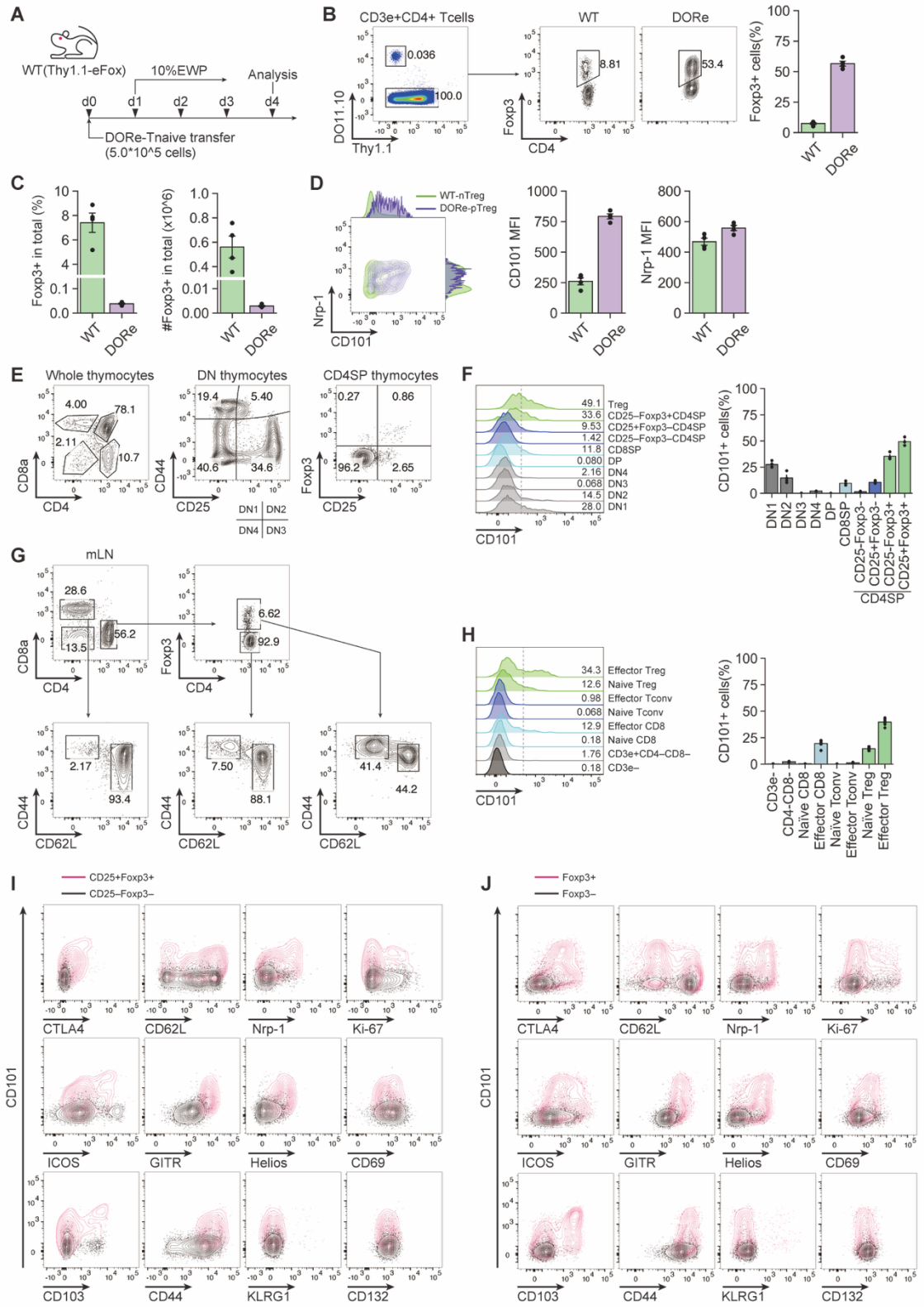
A
WT(Thy1.1-eFox)
10%EWP
Analysis
d0
d1
d2
d3
d4
DORe-Tnaive transfer
(5.0*10^5 cells)
B
CD3e+CD4+ Tcells
0.036
100.0
DO11.10
Thy1.1
WT
DORe
8.81
53.4
Foxp3
CD4
Foxp3+ cells(%)
C
Foxp3+ in total (%)
#Foxp3+ in total (x10^6)
D
WT-nTreg
DORe-pTreg
Nrp-1
CD101
CD101 MFI
Nrp-1 MFI
E
Whole thymocytes
DN thymocytes
CD4SP thymocytes
4.00
78.1
2.11
10.7
CD8a
CD4
19.4
5.40
40.6
34.6
CD44
CD25
DN1
DN2
DN4
DN3
0.27
0.86
96.2
2.65
Foxp3
F
49.1 Treg
33.6 CD25−Foxp3+CD4SP
9.53 CD25+Foxp3−CD4SP
1.42 CD25−Foxp3−CD4SP
11.8 CD8SP
0.080 DP
2.16 DN4
0.068 DN3
14.5 DN2
28.0 DN1
CD101+ cells(%)
DN1
DN2
DN3
DN4
DP
CD8SP
CD25−Foxp3−
CD25+Foxp3−
CD25−Foxp3+
CD25+Foxp3+
CD4SP
G
mLN
28.6
56.2
13.5
6.62
92.9
2.17
93.4
7.50
88.1
41.4
44.2
CD62L
H
34.3 Effector Treg
12.6 Naive Treg
0.98 Effector Tconv
0.068 Naive Tconv
12.9 Effector CD8
0.18 Naive CD8
1.76 CD3e+CD4−CD8−
0.18 CD3e−
CD3e−
CD4−CD8−
Naïve CD8
Effector CD8
Naïve Tconv
Effector Tconv
Naïve Treg
Effector Treg
I
CD25+Foxp3+
CD25−Foxp3−
CTLA4
CD62L
Nrp-1
Ki-67
ICOS
GITR
Helios
CD69
CD103
CD44
KLRG1
CD132
J
Foxp3+
Foxp3−

Fig. 5

1029

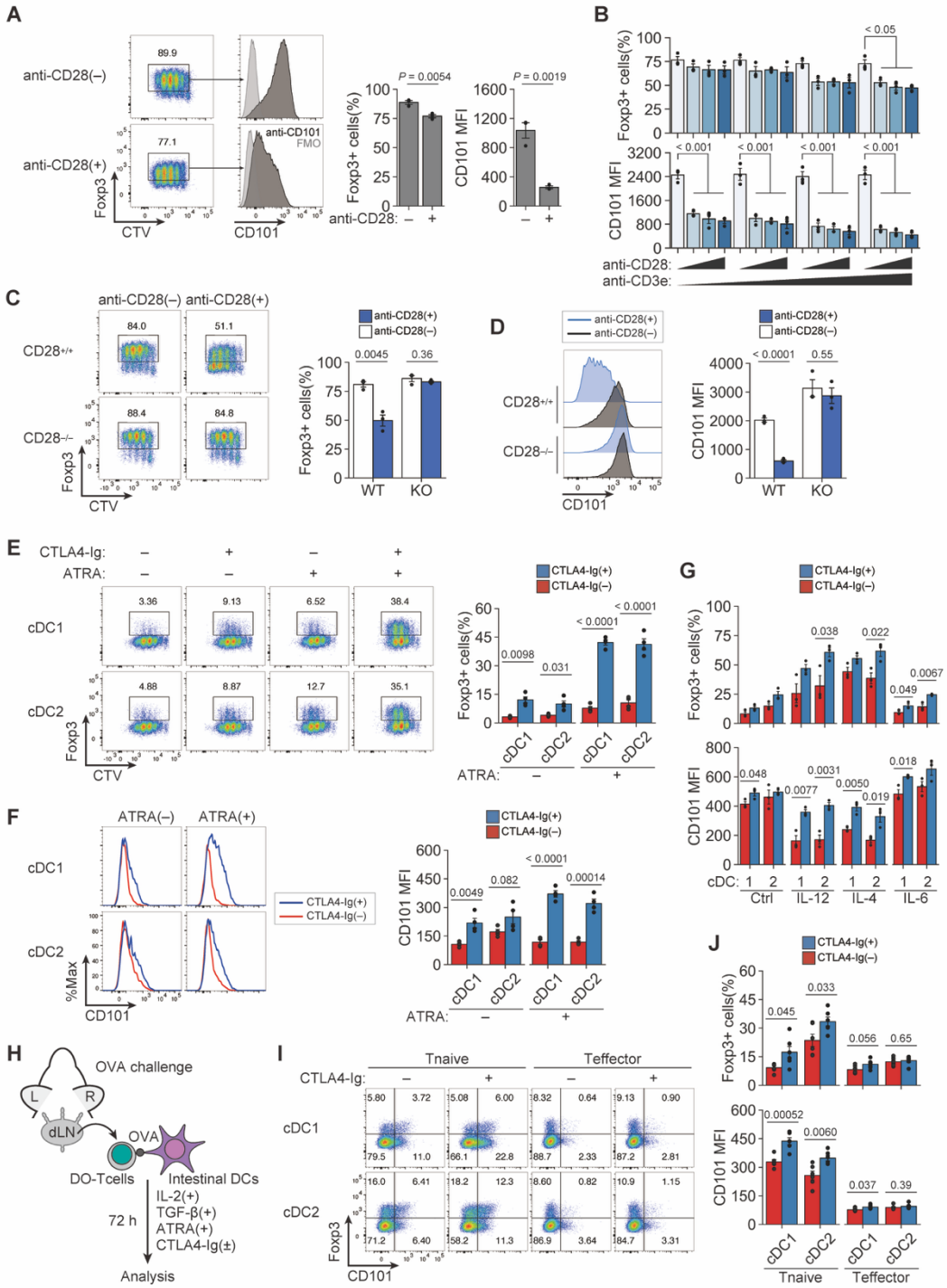
A
anti-CD28(–)
anti-CD28(+)
89.9
77.1
anti-CD101
FMO
Foxp3
CTV
CD101
P = 0.0054
P = 0.0019
Foxp3+ cells(%)
CD101 MFI
anti-CD28: – +
B
Foxp3+ cells(%)
CD101 MFI
< 0.05
< 0.001
anti-CD28:
anti-CD3e:
C
anti-CD28(–) anti-CD28(+)
CD28+/+
CD28–/–
84.0
51.1
88.4
84.8
anti-CD28(+)
anti-CD28(–)
0.0045
0.36
WT
KO
D
< 0.0001
0.55
E
CTLA4-Ig:
ATRA:
cDC1
cDC2
3.36
9.13
6.52
38.4
4.88
8.87
12.7
35.1
CTLA4-Ig(+)
CTLA4-Ig(–)
0.0098
0.031
< 0.0001
F
ATRA(–) ATRA(+)
%Max
0.0049
0.082
0.00014
G
0.038
0.022
0.049
0.0067
0.048
0.0077
0.0031
0.0050
0.019
0.018
cDC: 1 2 1 2 1 2 1 2
Ctrl IL-12 IL-4 IL-6
H
OVA challenge
L
R
dLN
OVA
DO-Tcells
Intestinal DCs
72 h
IL-2(+)
TGF-β(+)
ATRA(+)
CTLA4-Ig(±)
Analysis
I
Tnaive
Teffector
5.80 3.72 5.08 6.00 8.32 0.64 9.13 0.90
79.5 11.0 66.1 22.8 88.7 2.33 87.2 2.81
16.0 6.41 18.2 12.3 8.60 0.82 10.9 1.15
71.2 6.40 58.2 11.3 86.9 3.64 84.7 3.31
J
0.045
0.033
0.056
0.65
0.00052
0.0060
0.037
0.39

Fig. 6

1030

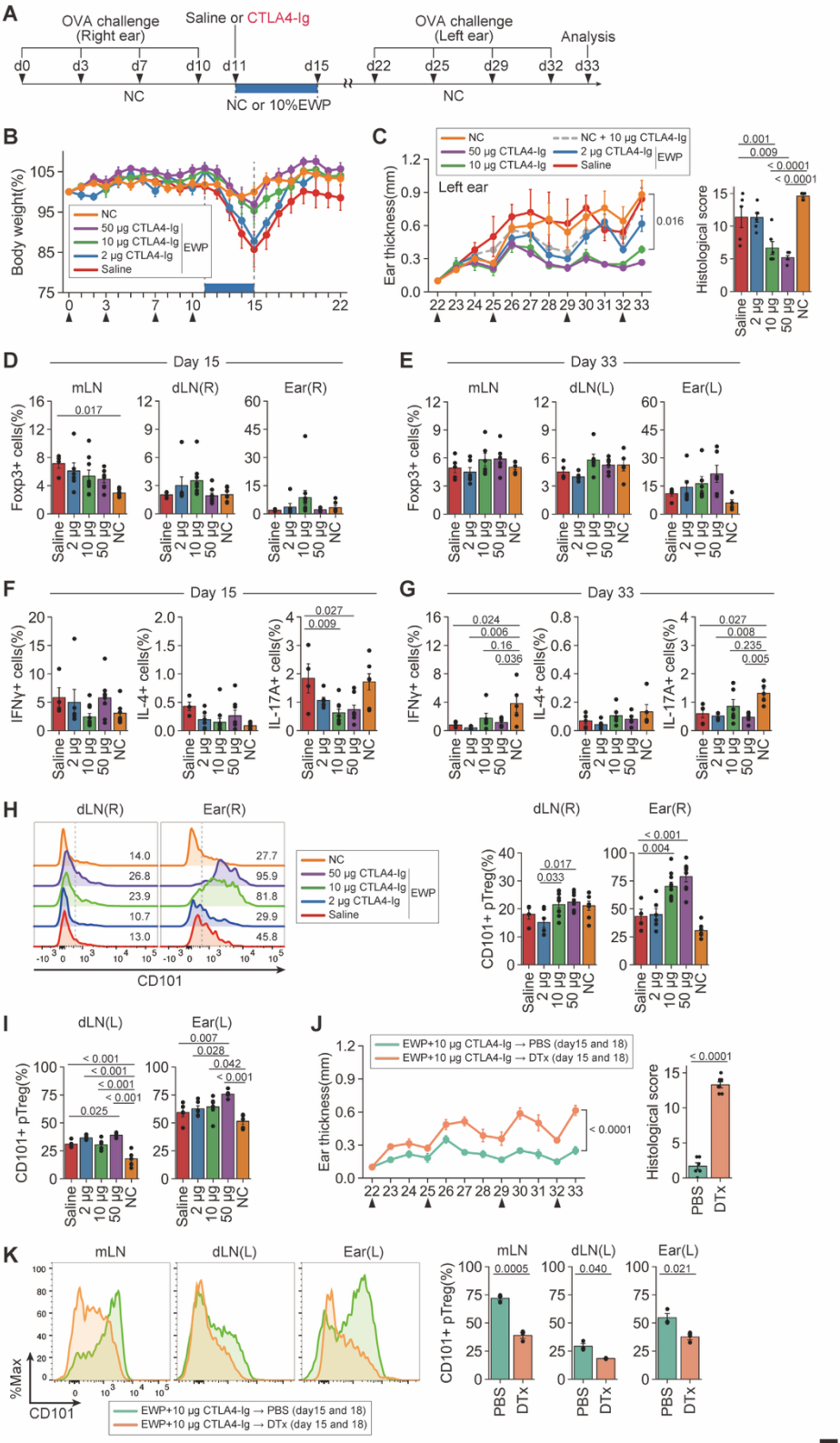
A
OVA challenge (Right ear)
Saline or CTLA4-Ig
OVA challenge (Left ear)
Analysis
d0 d3 d7 d10 d11 d15 d22 d25 d29 d32 d33
NC
NC or 10%EWP
NC
B
Body weight(%)
NC
50 μg CTLA4-Ig
10 μg CTLA4-Ig
2 μg CTLA4-Ig
Saline
EWP
C
Left ear
Ear thickness(mm)
NC + 10 μg CTLA4-Ig
Histological score
D
Day 15
mLN
dLN(R)
Ear(R)
Foxp3+ cells(%)
E
Day 33
dLN(L)
Ear(L)
F
IFNγ+ cells(%)
IL-4+ cells(%)
IL-17A+ cells(%)
G
H
CD101
CD101+ pTreg(%)
I
J
EWP+10 μg CTLA4-Ig → PBS (day15 and 18)
EWP+10 μg CTLA4-Ig → DTx (day 15 and 18)
PBS
DTx
K
%Max

Fig. 7

1031

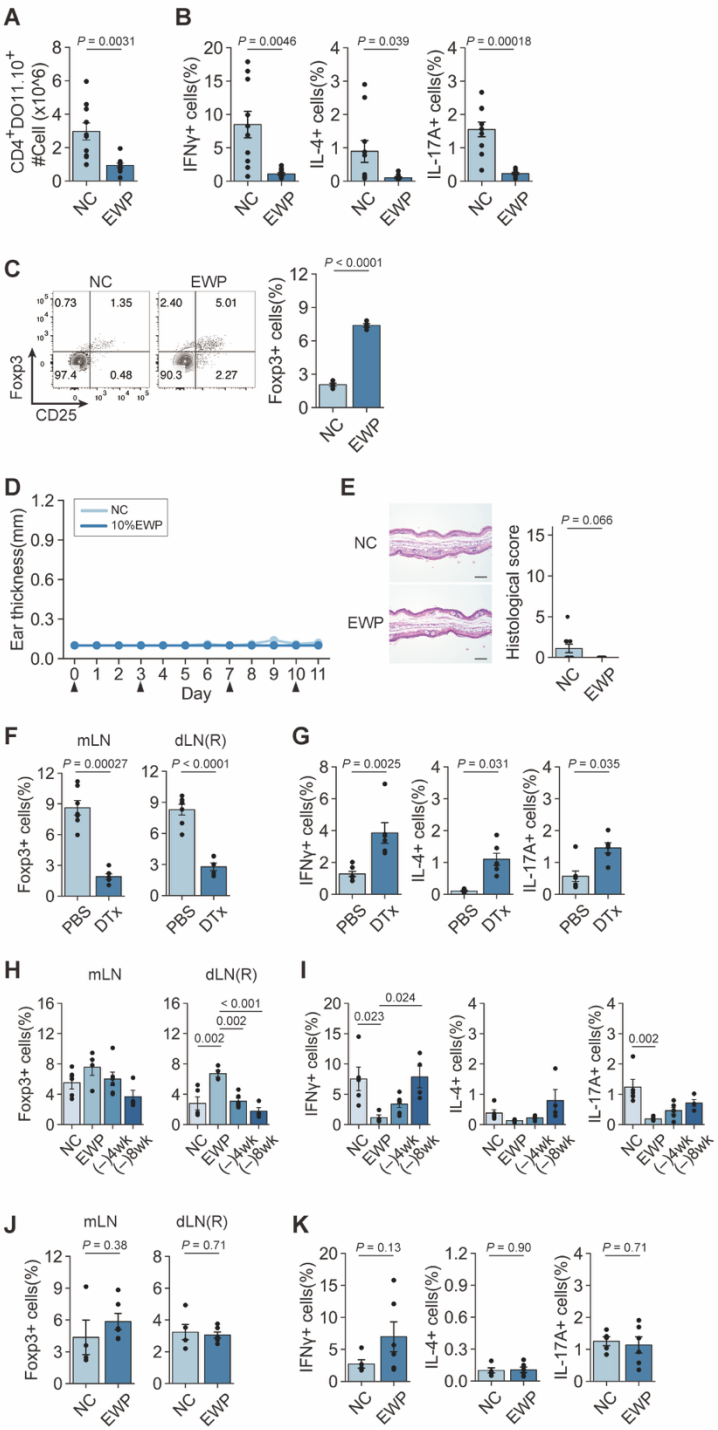
A
B
C
D
E
F
G
H
I
J
K
P = 0.0031
P = 0.0046
P = 0.039
P = 0.00018
P < 0.0001
P = 0.066
P = 0.00027
P = 0.0025
P = 0.031
P = 0.035
P = 0.38
P = 0.71
P = 0.13
P = 0.90
NC
EWP
PBS
DTx
mLN
dLN(R)
Day
Ear thickness(mm)
Histological score
Foxp3+ cells(%)
IFNγ+ cells(%)
IL-4+ cells(%)
IL-17A+ cells(%)
CD4+DO11.10+ #Cell (x10^6)
Foxp3
CD25
10%EWP
(−)4wk
(−)8wk

Fig. S1

1032

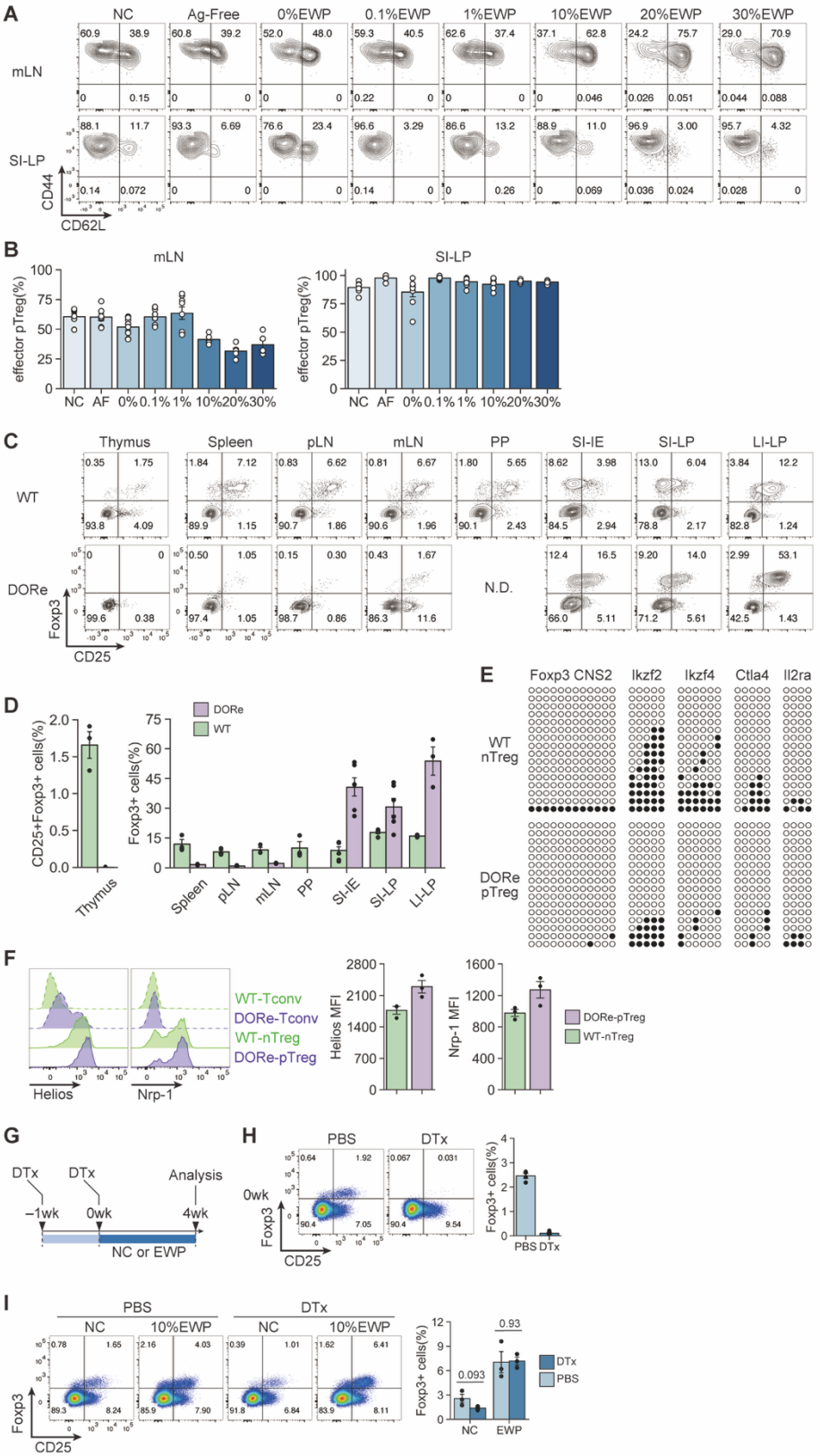
A
NC
Ag-Free
0%EWP
0.1%EWP
1%EWP
10%EWP
20%EWP
30%EWP
mLN
SI-LP
CD44
CD62L
B
mLN
SI-LP
effector pTreg(%)
NC AF 0% 0.1% 1% 10% 20% 30%
C
Thymus
Spleen
pLN
mLN
PP
SI-IE
SI-LP
LI-LP
WT
DORe
N.D.
Foxp3
CD25
D
DORe
WT
CD25+Foxp3+ cells(%)
Foxp3+ cells(%)
Thymus
Spleen
pLN
mLN
PP
SI-IE
SI-LP
LI-LP
E
Foxp3 CNS2
Ikzf2
Ikzf4
Ctla4
Il2ra
WT nTreg
DORe pTreg
F
WT-Tconv
DORe-Tconv
WT-nTreg
DORe-pTreg
Helios
Nrp-1
Helios MFI
Nrp-1 MFI
DORe-pTreg
WT-nTreg
G
DTx
DTx
Analysis
−1wk
0wk
4wk
NC or EWP
H
PBS
DTx
0wk
Foxp3
CD25
Foxp3+ cells(%)
PBS DTx
I
PBS
DTx
NC
10%EWP
NC
10%EWP
Foxp3
CD25
Foxp3+ cells(%)
0.093
0.93
NC
EWP
DTx
PBS

Fig. S2

1033

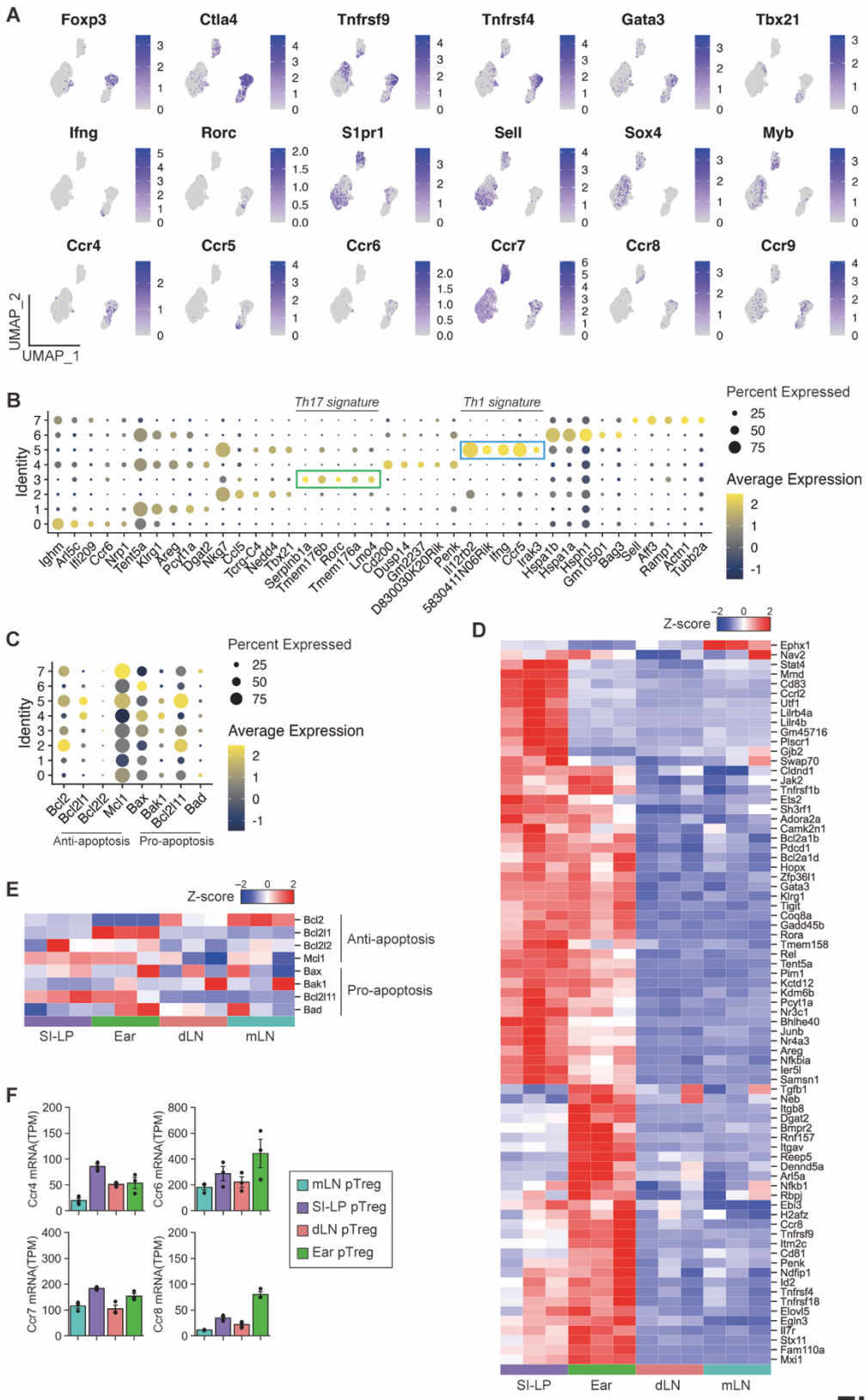
A
Foxp3
Ctla4
Tnfrsf9
Tnfrsf4
Gata3
Tbx21
Ifng
Rorc
S1pr1
Sell
Sox4
Myb
Ccr4
Ccr5
Ccr6
Ccr7
Ccr8
Ccr9
UMAP_2
UMAP_1
B
Th17 signature
Th1 signature
Percent Expressed
25
50
75
Average Expression
Identity
Ighm
Arl5c
Ifi209
Ccr6
Nrp1
Tent5a
Klrg1
Areg
Pcyt1a
Dgat2
Nkg7
Ccl5
Tcrg-C4
Nedd4
Tbx21
Serpinb1a
Tmem176b
Rorc
Tmem176a
Lmo4
Cd2001
Dusp14
Gm2237
D830030K20Rik
Penk
Il12rb2
5830411N06Rik
Ifng
Ccr5
Irak3
Hspa1b
Hspa1a
Hsph1
Gm10501
Bag3
Sell
Atf3
Ramp1
Actn1
Tubb2a
C
Percent Expressed
25
50
75
Average Expression
Identity
Bcl2
Bcl2l1
Bcl2l2
Mcl1
Bax
Bak1
Bcl2l11
Bad
Anti-apoptosis
Pro-apoptosis
D
Z-score
Ephx1
Nav2
Stat4
Mmd
Cd83
Ccrl2
Utf1
Lilrb4a
Lilr4b
Gm45716
Plscr1
Gjb2
Swap70
Cldnd1
Jak2
Tnfrsf1b
Ets2
Sh3rf1
Adora2a
Camk2n1
Bcl2a1b
Pdcd1
Bcl2a1d
Hopx
Zfp36l1
Gata3
Klrg1
Tigit
Coq8a
Gadd45b
Rora
Tmem158
Rel
Tent5a
Pim1
Kctd12
Kdm6b
Pcyt1a
Nr3c1
Bhlhe40
Junb
Nr4a3
Areg
Nfkbia
Ier5l
Samsn1
Tgfb1
Neb
Itgb8
Dgat2
Bmpr2
Rnf157
Itgav
Reep5
Dennd5a
Arl5a
Nfkb1
Rbpj
Ebi3
H2afz
Ccr8
Tnfrsf9
Itm2c
Cd81
Penk
Ndfip1
Id2
Tnfrsf4
Tnfrsf18
Elovl5
Egln3
Il7r
Stx11
Fam110a
Mxi1
SI-LP
Ear
dLN
mLN
E
Z-score
Bcl2
Bcl2l1
Bcl2l2
Mcl1
Bax
Bak1
Bcl2l11
Bad
Anti-apoptosis
Pro-apoptosis
SI-LP
Ear
dLN
mLN
F
Ccr4 mRNA(TPM)
Ccr6 mRNA(TPM)
Ccr7 mRNA(TPM)
Ccr8 mRNA(TPM)
mLN pTreg
SI-LP pTreg
dLN pTreg
Ear pTreg

Fig. S3

1034

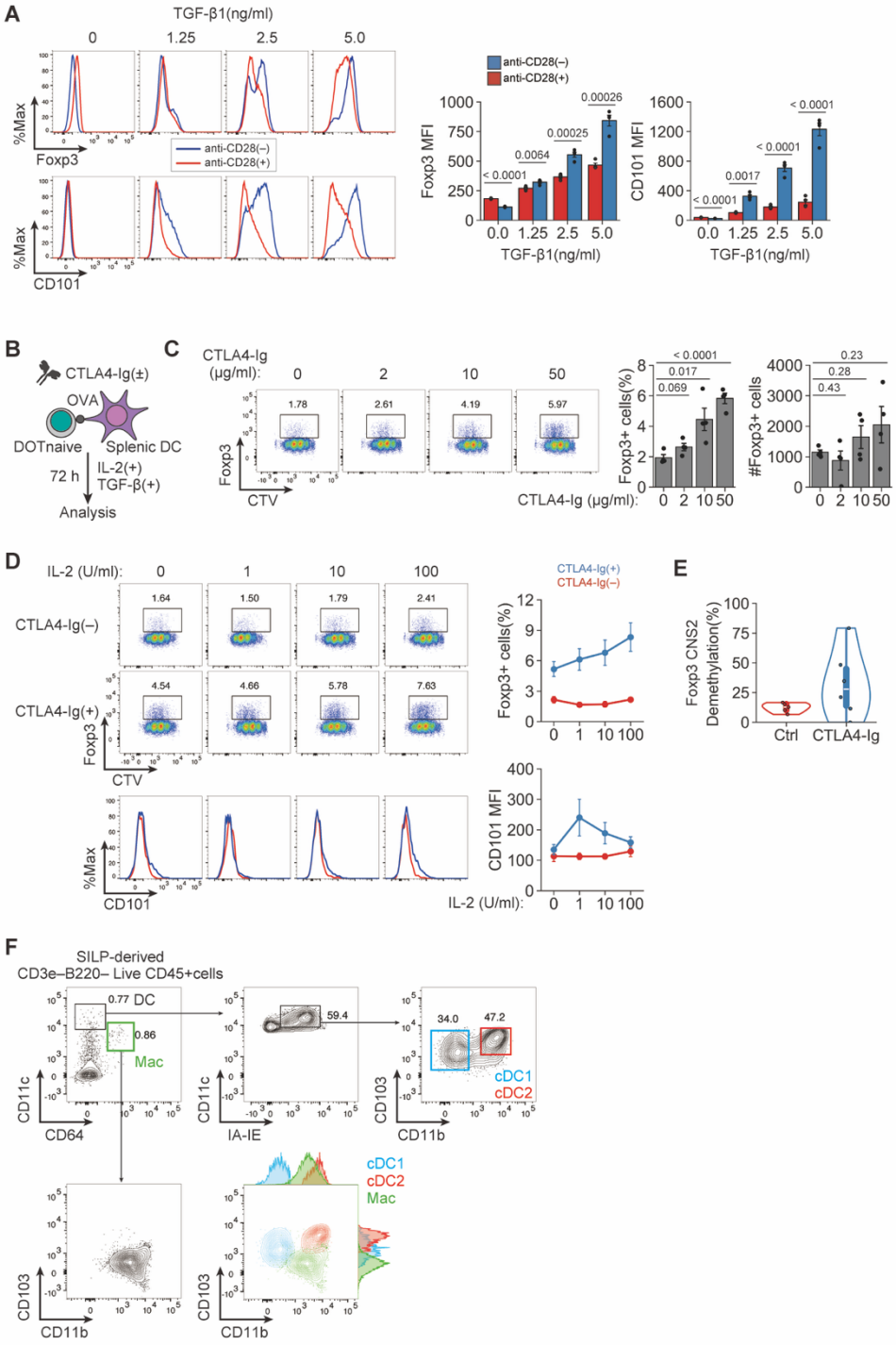
A
TGF-β1(ng/ml)
0
1.25
2.5
5.0
%Max
Foxp3
CD101
anti-CD28(–)
anti-CD28(+)
Foxp3 MFI
CD101 MFI
TGF-β1(ng/ml)
B
CTLA4-Ig(±)
OVA
DOTnaive
Splenic DC
72 h
IL-2(+)
TGF-β(+)
Analysis
C
CTLA4-Ig (μg/ml):
Foxp3+ cells(%)
#Foxp3+ cells
D
IL-2 (U/ml):
CTLA4-Ig(–)
CTLA4-Ig(+)
CTV
CD101 MFI
E
Foxp3 CNS2 Demethylation(%)
Ctrl
CTLA4-Ig
F
SILP-derived
CD3e–B220– Live CD45+cells
0.77 DC
0.86
Mac
59.4
34.0
47.2
cDC1
cDC2
CD11c
CD64
IA-IE
CD103
CD11b

Fig. S4

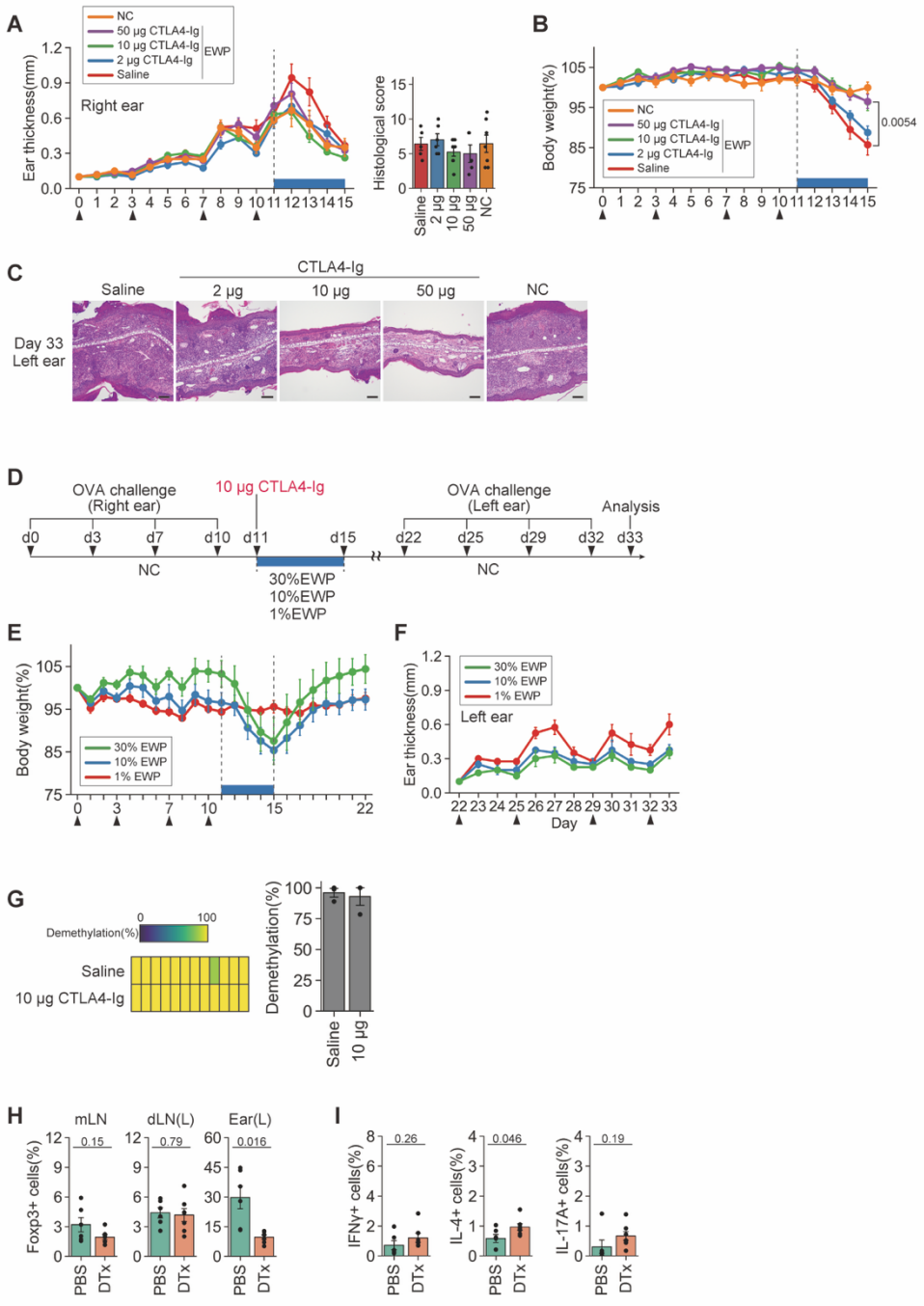
A
NC
50 μg CTLA4-Ig
10 μg CTLA4-Ig
2 μg CTLA4-Ig
Saline
EWP
Right ear
Ear thickness(mm)
Histological score
Saline
2 μg
10 μg
50 μg
NC
B
Body weight(%)
0.0054
C
CTLA4-Ig
Saline
2 μg
10 μg
50 μg
NC
Day 33
Left ear
D
OVA challenge
(Right ear)
10 μg CTLA4-Ig
OVA challenge
(Left ear)
Analysis
d0
d3
d7
d10
d11
d15
d22
d25
d29
d32
d33
NC
30%EWP
10%EWP
1%EWP
NC
E
Body weight(%)
30% EWP
10% EWP
1% EWP
F
Ear thickness(mm)
Left ear
Day
G
Demethylation(%)
Saline
10 μg CTLA4-Ig
Demethylation(%)
Saline
10 μg
H
mLN
dLN(L)
Ear(L)
Foxp3+ cells(%)
0.15
0.79
0.016
PBS
DTx
I
IFNγ+ cells(%)
IL-4+ cells(%)
IL-17A+ cells(%)
0.26
0.046
0.19
PBS
DTx

Fig. S5

1036

1037 **Table S1. Nutrition facts of modified food**

1038 CE-2 (Normal Chow; NC)

Nutrition facts	(%)
Water	8.84
Crude protein	25.48
Crude fat	4.61
Crude fiber	5.14
Crude ash	7.01
Nitrogen free extract	48.92
Total	100.00

1039 CE-2 (–)White fish powder (0%EWP)

Nutrition facts	(%)
Water	9.00
Crude protein	19.86
Crude fat	4.26
Crude fiber	5.30
Crude ash	6.24
Nitrogen free extract	55.34
Total	100.00

1040 Modified food

ID	CE-2 (–)White fish powder (%)	Corn starch (%)	EWP (%)	EWP derived protein (%)
0%EWP	100	0	0	0
0.1%EWP	99.89961	0.07743	0.02296	0.10000
1%EWP	98.99610	0.77431	0.22959	1.00000
10%EWP	89.96105	7.74300	2.29595	10.00000
20%EWP	79.92200	15.48609	4.59191	20.00000
30%EWP	69.88305	23.22909	6.88786	30.00000

1041

1042 **Table S2. List of antibodies**

1043 Antibodies used for flowcytometry, FACS sorting, and other experiments

Antibodies	Manufacturer	Identifier
Anti-mouse CD3e-APC (145-2C11)	BD pharmingen	Cat#553066; RRID: AB_398529
Anti-mouse CD3e-APC-Cy7 (145-2C11)	BioLegend	Cat#100330; RRID: AB_1877170
Anti-mouse CD3e-Biotin (145-2C11)	BD Biosciences	Cat#553060; RRID: AB_394593
Anti-mouse CD3e-PE (145-2C11)	Invitrogen	Cat#12-0031-82; RRID: AB_465496
Anti-mouse CD3e-V500 (500A2)	BD Biosciences	Cat#560771; RRID: AB_1937314
Anti-mouse CD4-AF700 (RM4-5)	Invitrogen	Cat#56-0042-82; RRID: AB_494000
Anti-mouse CD4-V500 (RM4-5)	BD Biosciences	Cat#560782; RRID: AB_1937327
Anti-mouse CD4-BV650 (RM4-5)	BD Biosciences	Cat#563747; RRID: AB_2716859
Anti-mouse CD8a-PerCP-Cy5.5 (53-6.7)	BD Biosciences	Cat#551162; RRID: AB_394081
Anti-mouse CD11b-AF700 (M1/70)	Invitrogen	Cat#56-0112-80; RRID: AB_657585
Anti-mouse CD11b-APC (M1/70)	BioLegend	Cat#101212; RRID: AB_312795
Anti-mouse CD11b-PerCP-Cy5.5 (M1/70)	Invitrogen	Cat#45-0112-82; RRID: AB_468714
Anti-mouse CD11c-BV605 (N418)	BIoLegend	Cat#117334; RRID: AB_2562415
Anti-mouse CD11c-PE-Cy7 (N418)	BioLegend	Cat#117318; RRID: AB_493568
Purified anti-mouse CD16/32 (93)	BioLegend	Cat#101302; RRID: AB_312801
Anti-mouse CD25-BV421 (PC61)	BioLegend	Cat#102034; RRID: AB_11203373
Anti-mouse CD25-PE (PC61)	BD pharmingen	Cat#553866; RRID: AB_395101
Anti-mouse CD25-PE-Cy7 (PC61)	BD Biosciences	Cat#552880; RRID: AB_394509
Anti-mouse CD25-PerCP-Cy5.5 (PC61)	BD Biosciences	Cat#551071; RRID: AB_394031
Anti-mouse CD44-APC (IM7)	Invitrogen	Cat#17-0441-83; RRID: AB_469390
Anti-mouse CD44-PE-Cy7 (IM7)	Invitrogen	Cat#25-0441-82; RRID: AB_469623
Anti-mouse CD44-V500 (IM7)	BD Biosciences	Cat#560780; RRID: AB_1937328
Anti-mouse CD45-BV510 (30-F11)	BioLegend	Cat#103138; RRID: AB_2563061
Anti-mouse CD45.1-APC-Cy7 (A20)	BioLegend	Cat#110716; RRID: AB_313505
Anti-mouse/human CD45R/B220-APC-eFluor780 (RA3-6B2)	Invitrogen	Cat#47-0452-82; RRID: AB_1518810
Anti-mouse/human CD45R/B220-Biotin (RA3-6B2)	BioLegend	Cat#103204; RRID: AB_312989
Anti-mouse CD62L-BV421 (MEL-14)	BD Biosciences	Cat#562910; RRID: AB_2737885
Anti-mouse CD62L-PerCP-Cy5.5 (MEL-14)	BD pharmingen	Cat#560513; RRID: AB_10611578
Anti-mouse CD64-PE (X54-5/7.1)	BioLegend	Cat#139304; RRID: AB_10612740
Anti-mouse CD90.1-BV605 (OX-7)	BD Biosciences	Cat#740374; RRID: AB_2740106
Anti-mouse CD90.1-PerCP (OX-7)	BD Biosciences	Cat#557266; RRID: AB_396611
Anti-mouse CD90.2-AF700 (53-2.1)	BioLegend	Cat#140324; RRID: AB_2566740
Anti-mouse CD90.2-PE-Cy7 (53-2.1)	BioLegend	Cat#140310; RRID: AB_10643586
Anti-mouse CD101-APC (REA301)	Miltenyi Biotec	Cat#130-104-304; RRID: AB_2654344
Anti-mouse CD101-PE (REA301)	Miltenyi Biotec	Cat#130-120-173; RRID: AB_2752032
Anti-mouse CD101-PE-Vio770 (REA301)	Miltenyi Biotec	Cat#130-104-305; RRID: AB_2654345

Anti-mouse CD103-APC (2E7)	Invitrogen	Cat#17-1031-82; RRID: AB_1106992
Anti-mouse CD103-PE-Cy7 (2E7)	BioLegend	Cat#121426; RRID: AB_2563691
Anti-mouse CD134(OX40)-BV421 (OX-86)	BioLegend	Cat#119411; RRID: AB_10962569
Anti-mouse CD134(OX40)-PE (OX-86)	BioLegend	Cat#119410; RRID: AB_2207344
Anti-mouse CD137(4-1BB)-APC (17B5)	BioLegend	Cat#106110; RRID: AB_2564297
Anti-mouse CD195(CCR5)-BV421 (C34-3448)	BD Biosciences	Cat#743695; RRID: AB_2741677
Anti-mouse CD199(CCR9)-PE (CW-1.2)	BioLegend	Cat#128710; RRID: AB_1227479
Anti-mouse CD278(ICOS)-PE-Cy7 (C398.4A)	BioLegend	Cat#313520; RRID: AB_10643411
Anti-mouse CD304(Neuropilin-1)-eFluor450 (3DS304M)	Invitrogen	Cat#48-3041-82; RRID: AB_2574051
Anti-mouse CD304(Neuropilin-1)-PE-Cy7 (3DS304M)	Invitrogen	Cat#25-3041-82; RRID: AB_2573436
Anti-mouse CD357(GITR)-PE-Cy7 (DTA-1)	BD Biosciences	Cat#558140; RRID: AB_647252
Anti-mouse/human Helios-APC (22F6)	BioLegend	Cat#137218; RRID: AB_10660750
Anti-mouse/human Helios-PE-Cy7 (22F6)	BioLegend	Cat#137236; RRID: AB_2565990
Anti-mouse I-A/I-E-BV421 (M5/114.15.2)	BioLegend	Cat#107631; RRID: AB_10900075
Anti-mouse I-A/I-E-BV510 (M5/114.15.2)	BioLegend	Cat#107635; RRID: AB_2561397
Anti-mouse/human Ki-67-PE-Cy7 (SolA15)	Invitrogen	Cat#25-5698-82; RRID: AB_11220070
Anti-mouse/human KLRG1-PerCP-Cy5.5 (2F1/KLRG1)	BioLegend	Cat#138418; RRID: AB_2563014
Anti-mouse/human T-bet-BV421 (4B10)	BioLegend	Cat#644816; RRID: AB_2686976
Anti-mouse TCR DO11.10-APC (KJ1-26)	Invitrogen	Cat#17-5808-80; RRID: AB_469459
Anti-mouse TCR DO11.10-PerCP-Cy5.5 (KJ1-26)	BioLegend	Cat#118512; RRID: AB_2028522
Anti-mouse TER-119/Erythroid Cells-Biotin (TER-119)	BD pharmingen	Cat#553672; RRID: AB_394985
Anti-mouse TIGIT-APC (1G9)	BioLegend	Cat#142105; RRID: AB_10960139
Anti-mouse Foxp3-Alexa Fluor 488 (FJK-16s)	Invitrogen	Cat#53-5773-82; RRID: AB_763537
Anti-human/mouse Gata3-eFlour660 (TWAJ)	Invitrogen	Cat#50-9966-42; RRID: AB_10596663
Anti-mouse RORgamma(t)-PE (B2D)	Invitrogen	Cat#12-6981-82; RRID: AB_10807092
Anti-mouse IL-4-APC (11B11)	Invitrogen	Cat#17-7041-82; RRID: AB_469494
Anti-mouse IL-17A-BV421 (TC11-18H10.1)	BioLegend	Cat#506925; RRID: AB_10900442
Anti-mouse IFN gamma-PE (XMG1.2)	Invitrogen	Cat#12-7311-82; RRID: AB_466193
TotalSeq-C0301 anti-mouse Hashtag 1 Antibody	BioLegend	Cat#155861; RRID: AB_2800693
TotalSeq-C0302 anti-mouse Hashtag 2 Antibody	BioLegend	Cat#155863; RRID: AB_2800694
TotalSeq-C0303 anti-mouse Hashtag 3 Antibody	BioLegend	Cat#155865; RRID: AB_2800695
TotalSeq-C0304 anti-mouse Hashtag 4 Antibody	BioLegend	Cat#155867; RRID: AB_2800696
Purified NA/LE anti-mouse CD3e (145-2C11)	BD pharmingen	Cat#553057; RRID: AB_394590
Purified NA/LE anti-mouse CD28 (37.51)	BD pharmingen	Cat#553294; RRID: AB_394763
Anti-Histone H3 Acetyl Lys27	GeneTex	Cat#GTX60815; RRID: AB_2888004

1044